Investigation of the Influence of Microgravity on Transport Mechanisms in a Virtual Spaceflight Chamber

— A Ground-Based Program —

Contract No.: NAS8-40848

FINAL REPORT
Period of Performance:
06/04/96 to 12/03/00

Prepared on March 20, 2001

Prepared by:

James D. Trolinger, Principal Investigator
MetroLaser, Inc.
18010 Skypark Circle, Suite 100
Irvine CA 92614
E-mail: jtrolinger@metrolaserinc.com

and

Co-Investigators:

Dr. Ravindra B. Lal
Alabama A&M University
Dept. of Physics, Rm. 145
Chambers Hall, Meridian St.
Normal, AL 35762
(205) 851-5309

Professor Roger Rangel
University of California Irvine
Dept. of Mechanical & AeroSpace Eng.
Irvine, CA 92697
(949) 824-4033

William Witherow and Jan Rogers
Marshall Spaceflight Center
M/S ES74 SSL Bldg. 4481
Huntsville, AL 35812
(205) 544-7811

TABLE OF CONTENTS

TABLE OF FIGURES

Figure **Page**

LIST OF ABBREVIATIONS AND ACRONYMS

ABBREVIATIONS

A	Velocity amplitude (**a** is dimensionless)
a	Radius of the particle
$\mathbf{f}_H$	History force
$\mathbf{f}_{St}$	Stokes force
$\mathbf{f}_{VM}$	Virtual mass force
g	Local gravity acceleration
G	Gravitational coefficient $(1-\alpha)\,\tau_p\,\mathbf{g}/U_o$
k	Virtual mass coefficient $2/(2+\alpha)$
Re_p	Particle Reynolds number $a\mathbf{W}/\nu$
S	Scaling number $\frac{\alpha\omega}{2} = \frac{\Omega}{\nu}\left(\frac{a}{3}\right)^2$
t	Time ($\hat{t}$ is dimensionless)
U	Fluid velocity (**u** is dimensionless)
V	Particle velocity (**v** is dimensionless)
W	Relative velocity **V** – **U** (**w** is dimensionless)
α	Fluid-to-particle density ratio
α_c	Fluid-to-particle density ratio at which solution character changes, 8/5
f	Particle-to-fluid phase difference
η	Particle-to-fluid amplitude ratio $(1 + b_i / a_i)$
μ	Dynamic viscosity
μM	Micron- $1X10^{-6}$ meters
ν	Kinematic viscosity
ρ	Density
τ_p	Characteristic time $2\rho_p a^2/9\mu$
Ω	Angular frequency of the fluid surrounding the particle
ω	Dimensionless angular frequency $= \Omega\tau_p$

ACRONYMS

CCD	Charge Coupled Device
IML-1	International Microgravity Laboratory #1 - Spaceflight experiment flown in 1995
FES	Fluids Experiment System
MAMS	Microgravity Acceleration Measurement System
OARE	Orbital Acceleration Research Experiment
PAS	Passive Acceleration System
SAMS	Space Acceleration Measurement System
SL3	Space Laboratory #3 - Spaceflight experiment flown in April of 1985
TGS	Triglycine Sulfate
USML-1	First United States Microgravity Laboratory

ABSTRACT

The IML-1 Spaceflight produced over 1000 holograms of a well-defined particle field in the low g Spacelab environment; each containing as much as 1000 megabytes of information. This project took advantage of these data and the concept of holographic "virtual" spaceflight to advance the understanding of convection in the space shuttle environment, g-jitter effects on crystal growth, and complex transport phenomena in low Reynolds number flows. The first objective of the proposed work was to advance the understanding of microgravity effects on crystal growth. This objective was achieved through the use of existing holographic data recorded during the IML-1 Spaceflight. The second objective was to design a spaceflight experiment that exploits the "virtual space chamber concept" in which holograms of space chambers can provide a virtual access to space. This led to a flight definition project, which is now underway under a separate contract known as SHIVA, Spaceflight Holography Investigation in a Virtual Apparatus.

BACKGROUND

In January 1992, the IML-1 FES experiment produced a set of classic experimental data and a 40 hour holographic "movie" of an ensemble of spheres in a fluid in microgravity. Because the data are in the form of holograms, we can study the three-dimensional distribution of particles with unprecedented detail by a variety of methods and for a wide variety of interests. The possession of the holographic movie is tantamount to having a complex experiment in space while working in an easily accessible laboratory on earth. The movie contains a vast amount of useful data, including residual g, g-jitter, convection and transport data, and particle fluid interaction data. The information content in the movie is so great that we have scarcely begun to tap into the data that is actually available in the more than 1000 holograms, each containing as much as 1000 megabytes of information. This has shed new light on the effects of microgravity on materials processing.

The types of information extractable from these holograms has improved our understanding of the microgravity environment, thereby allowing NASA to better exploit its use in such applications as crystal growth from solution. The early part of this investigation made extensive use of existing holographic data produced in the IML-1 experiment. The further analysis of this data provided the basis for a breadboard that was built and used in ground-based experiments.

The history of the project dates back to 1986 when (unexpected) free-floating crystalline particles were observed in holographic data from Spacelab 3 during a crystal-growth-from-solution experiment. (See cover picture.) A few particles were tracked holographically for many hours. We realized that crude estimates of residual gravity and g-jitter could be made from these data when used in conjunction with the equations of motion of a particle in a fluid. Also, direct observation of microconvection was made and would be quantifiable if the particles followed the flow precisely. In these and subsequent experiments, we used the methods for quantifying microconvection and the microgravity environment around the crystal, and we fully recognized the potential of holographically recording the data.

The Spacelab 3 holographic data represents the first direct observation of a diffusion (depletion) layer in diffusion-limited crystal growth in space on both a fixed crystal as well as a free floating

crystal (see cover figure). Moreover, the effect on crystal growth of the motion of the crystal through the fluid was observed directly.

We realized that to make the quantitative data accurate would require additional terms (that were usually neglected and usually negligible in a gravity field) in the particle equation of motion in a fluid. Coimbra and Rangel, who were working on particle/fluid mechanics problems, joined the team to provide the needed analytical support. They developed, for the first time, an analytical solution of the equations that had previously been solvable only by numerical methods. In 1996, a ground-based program was awarded to further develop the "virtual (spaceflight) apparatus" concept, and to use the methods developed to exploit fully the IML-1 data.

Further analysis of the analytical solutions led us to the conclusion that the most significant deviation from the traditional solutions will be easiest to quantify and observe in a microgravity environment. The reason is that gravity usually dominates the longer-term solution, masking the other effects that can take place in a short-term. Predictions and models of materials sciences experiments based on the traditional solutions to the equation of motion of a particle would be incorrect in microgravity for some easily measurable phenomena. This led to a flight definition experiment to test the new solutions, which was awarded in 1998.

OBJECTIVES

The first objective of the proposed work was to advance the understanding of microgravity effects on crystal growth, convection in materials processing in the Space Shuttle environment, and complex transport phenomena at low Reynolds numbers. This objective was achieved through the use of existing holographic data recorded during the IML-1 Spaceflight. Much of the convection present in these recordings is connected with thermal and concentration gradients related to crystal growth driven by g-jitter, residual g, and other sources. The program produced important crystal-growth-in-space data never before obtainable from existing hardware, and provided direct measurements of the microgravity environment that have been unattainable to date with existing flight hardware.

The second objective was to design a spaceflight experiment that exploits the "virtual space chamber concept". The work led to a flight definition experiment, now underway under a separate contract, that has already moved successfully past the Science Concept Review stage and into the requirements definition phase. We anticipate that the flight program will provide data that takes us closer to a fundamental understanding of microgravity and its affect on materials processing.

VIRTUAL SPACEFLIGHT CHAMBER CONCEPT

Certain spaceflight experiments can be recorded in holograms in such a manner that having the holograms on earth is optically equivalent to being back in space with unlimited time to view the experiment. Properly exploited, this concept can save a significant amount of experiment time in space by effectively bringing the experiment optically back to earth.

Approach

Our technical approach was designed to exploit existing NASA spaceflight data and hardware to provide knowledge about microgravity influences in materials processing. This knowledge was used to design a new spaceflight experiment and hardware that would be superior to any existing

flight hardware in its capabilities to both monitor critical crystal growth parameters and directly measure microgravity effects such as residual gravity and g-jitter.

We exploited existing holograms recorded during the IML-1 Spaceflight in the following way:

1. Used existing data extraction/reduction capability.
2. Extracted additional data for g-jitter, transport properties, and particle interaction.
3. Used knowledge gained from the IML-1 data to produce design data for new chamber.
4. Developed a simplified, holographically-instrumented crystal growth concept for potential flight experiment.

Tasks

The following tasks made up the work:

1. **Produce an inventory and prioritize the value of data relevant to materials processing in space that potentially exists in the IML-1 holograms.**
2. **Extract additional supporting data for measurements, conclusions, and unanswered questions that have already resulted from the IML-1 holograms.**
   a. More complete data in z-axis.
   b. Regions not previously explored.
   c. Views not previously explored.
   d. Secondary holocamera views.
3. **Examine additional data types from IML-1 holograms not already considered.**
   a. Three-dimensional convection map as a function of time and event parameters.
   b. Individual particles with large separation distance from other particles that are out of the range of influence.
   c. Ensembles of particles close to one another but isolated from other particles within a range of interactive influence.
   d. Particles in clusters containing all three sizes of particles that were used in IML-1.
   e. Particle doublets that can be used for rotation and vorticity measurement.
   f. Particles near walls exhibiting wall influence.
   g. Particles exhibiting unusual motion.
   h. Particles near the crystal surface.
4. **Analyze and interpret IML-1 data.**
   a. Support existing measurements and conclusions.
   b. Correlate convection to temperature and concentration gradients and shuttle attitude.
   c. Refine fluid models to incorporate observed phenomena.
   d. Explain unexpected, long-term persistence of convection.
   e. Resolve other previously unanswered questions.
   f. Provide new understanding of convection in the space shuttle environment in materials processing experiments.

5. **Produce a preliminary experiment design which consists of:**
   a. Acceleration measurements.
   b. Microgravity measurements (residual gravity/g-jitter) using holographic PIV.
   d. Crystal growth monitoring.
   e. Particle movement with force field.
   f. Preliminary selection of crystal, fluid, and particle type/size.
6. **Produce a preliminary instrument design.**
   a. Select chamber type and size.
   b. Holocamera.
   c. Crystal growth hardware.
   d. Incorporate existing particle tracking data reduction system into the proposed requirement.
   e. Select individual components.
   f. Optimize the cell for crystal-growth-in-space research.
   g. Design the cell mounting and temperature control system.
   h. Select the control computer.
7. **Model the proposed instrument.**
   a. Reduce the equations of motion to the applicable set.
   b. Conduct computer experiments to optimize component choice.
   c. Determine anticipated instrument requirements.
   d. Specify instrument design parameters.
   e. Perform and apply a full error analysis accounting for all relevant variables.
   f. Incorporate results of the error analysis into the design.
8. **Breadboard and test the instrument.**
   a. Assemble the optical breadboard to provide a test bed for instrumentation development.
   b. Test for spatial resolution.
   c. Confirm optimum component selection.
   d. Select and use high viscous liquid to simulate microgravity effects.
   e. Introduce chosen crystal and particles.
   f. Test data reduction procedures.
   g. Produce final design information.
9. **Perform ground crystal growth demonstration.**
   a. Record holograms of crystal growth incorporating particles with g-jitter simulation.
   b. Characterize and evaluate the system capability.
   c. Identify critical issues and problems in using the instrument concept's space shuttle experiments.
10. **Design a flight package to include:**
    a. Housings.
    b. Controls.
    c. Diagnostics.
11. **Produce final report and recommendations.**

SUMMARY OF THEORETICAL WORK

In the equation of motion of a particle in a fluid, some of the terms that are almost always negligible in a gravitational field will become important in microgravity. One term, the history term, is almost always neglected in analyses and experiments, partly because it is extremely difficult to deal with analytically. Computations in the past have always been numerical. Team members, Coimbra and Rangel, discovered an analytical solution to the equation (a landmark discovery). They applied the work to specific cases of interest for this program and have provided data to support potential flight experiments.

Our solution shows that the history term cannot be neglected for many interesting cases (especially low Reynolds number cases). Most of these cases cannot be tested in a gravitational field because the particles fall to the bottom of the chamber or rise to the top. Coimbra and Rangel exploited the solution and looked for cases of interest.

The solutions to the equations helped us to identify parameters for a future spaceflight experiment. It was shown that a narrow range of experiments could be run on the ground to test a small part of the solution. The case where the fluid density is ½ the particle density and the particles are as large as 2 mm in diameter or larger will show the history effects to a measurable extent before they rise to the top.

SUMMARY OF EXPERIMENTAL WORK

We completed tasks to support the original goals and also conducted experimental work to support the flight program. This included the following:

1. Moved core part of the holographic ground reconstruction system (HGS) from MSFC to MetroLaser.
2. Set up reconstruction system at MetroLaser:
   a. Computer controlled traversing system.
   b. Vacuum platen for IML-1 holograms.
   c. Microscope re-imaging of reconstructed image.
   d. Frame grabber and TV camera.
   e. Image processing system.
3. Developed and/or integrated existing software for holographic data extraction from IML-1 holograms:
   a. Programmable traversing through the sample volume.
   b. Automated frame-grabbing at selected intervals.
   c. Filtering image to improve particle image quality.
   d. Numbering and locating particles.
   e. Evaluating quality of each particle image in each frame.
4. Developed and integrated software for image processing:
   a. Locate best focus plane.
   b. Determine the environment of each particle (i.e., how close is nearest particle?).
5. Developed and integrated software for particle tracking:
   a. Locate a particle of a specific size, environment, and location.
6. Scanned selected IML-1 holograms and produced a complete database of particles.
7. Developed software and methods to precisely register two related holograms.

8. Developed software to locate particles precisely in the 3-D image.
9. Developed a procedure to integrate the spaceflight experiment with the g-LIMIT isolation system.
10. Refined the reconstruction system to allow automatic scanning in all three dimensions.
11. Designed a KC-135 experiment with Dr. Jan Rogers and William Witherow.
12. Conducted a KC-135 particle holography experiment.
13. Evaluated KC-135 flight data.
14. Installed and tested 3-D scanning system for the HGS.
15. Scanned holograms to increase the database.
16. Mapped motions of particles with and without nearby particle influence.
17. Software for the reconstruction system and image analysis was completed and became operational.
18. Archived all particle field position data from IML-1 on CDs, making this database available to universities and researchers for additional data analysis.
19. Designed a ground-based experiment for particle movement.
20. Designed a spaceflight experiment.
21. Presented progress at the Materials Science Conference in July 1998 and June 2000.
22. Evaluated wavefront procedures for concentration measurement.
23. Developed a tether method to simulate microgravity effects.
24. Identified other types of data available in the holograms and examined ways of extracting it.
25. Identified the types of data that may have been missing from IML-1 data that should be incorporated into future test chambers.
26. A real-time phase shift interferometer was set up and adapted to view the wavefronts from the IML-1 type of data. The breadboard data reduction system developed for this purpose was used to view crystals growing in a solution. The changing contour of the crystal surface could be mapped.
27. Compared ground data with theoretical predictions.

A no-cost extension was requested and granted to allow the work on this project to be coordinated with, and to support, the related flight definition program. The effort was concentrated on the development of procedures that would lead to more accurate data reduction. A new cell was designed and new procedures were devised to improve the accuracy of location of a particle in the reconstructed image.

THEORY OF PARTICLE MOVEMENT IN FLUIDS AT LOW REYNOLDS NUMBER

Studies of particle trajectories in multidimensional flows are among the highest priorities in the field of Fluid Dynamics. Access to microgravity provides an opportunity to experimentally study types of particle motion that are negligible or difficult to observe where gravity forces dominate. Particles suspended in a fluid in microgravity move under a variety of forces associated with residual microgravity and its fluctuations due to orbital position, movement in the Space station, thrusters that adjust the attitude of the spacecraft, machinery, and residual convection associated with density gradients and crystal growth. Examination of the general equation of motion for the particles in this study has enabled us to determine which terms in the equation would be important in microgravity, what accuracy would be required of the diagnostics, and how to improve both the accuracy and the dynamic range of the measurement.

During the theoretical effort, we developed a procedure to solve the equation exactly (to the approximations made in the derivation of the equation) for a generic, uniform flow field $\mathbf{U}(t) \neq 0$.

This was accomplished by applying a fractional differential operator to a dimensionless form of the particle equation of motion. This procedure yields a second-order, explicit, differential equation in the relative particle-to-fluid velocity. During the derivation of the explicit equation, attention is given to the identification of the terms in this equation with the original forces that generate them. The resulting linear, non-homogenous, second-order ordinary equation is then solved exactly using variation of parameters.

The first relevant contribution to the study of forces acting on immersed objects in a viscous fluid is due to Stokes (1845)[1]. Stokes derived the famous expression for the steady-state drag acting on a small sphere that is subjected to a constant free-stream flow velocity. The Stokes drag force formula relates the force exerted on the sphere to the free-stream velocity, the viscosity of the fluid and diameter of the sphere in a linear way, given that the particle Reynolds number (Re_p) is maintained at much smaller than 1. In fact, the Stokes drag happens to agree well with experiments for values of Re_p up to 1, but this coincidental fact should not be generally extrapolated to unsteady flows. However, recent numerical evidence suggests that neglecting the convective contribution to the force acting on a small particle results in a small error for oscillating flows at high Strouhal number even for Re_p larger than 1 (Kim et al., 1998[2]). Stokes also showed that the drag force in this particular case (steady flow around a small sphere) is composed of 2/3 shear stresses and 1/3 pressure gradient on the surface of the sphere. The linear functional form of the Stokes drag on the far-field velocity ($\mathbf{F}_{St} = 6\pi a \mu U_\infty$) is preserved even when the particle is not solid and presents internal circulation. In this case, a multiplicative correction term that relates the strength of the internal circulation due to the different viscosity of the drop modifies the viscosity factor (Rybczynski, 1911[3]; Hadamard, 1911[4]). Implicit in Stokes'

---

1 G.G. Stokes, "On the theories of internal friction of fluids in motion." Trans. Cambridge Philos. Soc., 8, 287-305 (1845).

2 I. Kim, S. Elghobashi, and W.A. Sirignano "On the equation for spherical particle motion: effects of Reynolds and acceleration numbers." *J. Fluid. Mech.*, 367, pp. 221-253, (1998).

3 W. Rybczynski, "Uber die fortschreitende Bewegung einer Flussigen Kugel in einem zahen Medium." Bull. Int. Acad. Sci. Cracov., 1911A, pp. 40-46 (1911).

derivation is the premise that the particle is not accelerating with respect to the free-stream velocity. In the gravitationally-induced motion through a quiescent fluid, the free-stream velocity is constant (zero) but the particle accelerates until it reaches its terminal velocity. In this case, and in many others of practical interest, the quasi-steady formulation of the problem incurs an error and the unsteady contribution from the developing profile near the particle needs to be taken into account.

Almost half a century after Stokes derived his famous drag expression, attention was turned to solving the unsteady diffusion equation around a particle in an infinite medium. This problem was first tackled by Boussinesq (1885)[5] and by Basset (1888)[6], specifically for the gravitationally-induced motion of a small particle in a viscous fluid. The resulting expression obtained by consideration of the time-dependent evolution of the near-particle velocity profiles includes a term that is commonly called the Basset or history drag force. Evidence suggests that Boussinesq derived the form of the history drag first (Michaelides[7] and Feng[8], 1994), so the terminology 'history' or 'unsteady' drag is favored in this work.

Oseen (1927[9]) compiled and contributed to the previous work of Boussinesq and Basset, concentrating (with little success) on the extension of the previous equations to higher Re_p numbers. The particle equation of motion with a constant forcing (the gravity term) is usually referred to as the BBO equation, due to the original contributions of Boussinesq, Basset and Oseen. The BBO equation is an integro-differential equation that has a removable singularity at the current time in the integrand of the history term.

The history drag term makes the particle equation of motion integro-differential, and thus more difficult to solve than the previous (quasi-steady) ordinary differential equation. Boggio (1927)[10] inverted the equation to derive the exact velocity history of a small particle moving under the influence of gravity in an otherwise quiescent fluid. This classical result remained the only closed form solution of the unsteady motion of a small particle in suspension. The main reason

---

4 J. Hadamard, "Movement permanent lent d'une sphère liquide visqueuse dans un liquid visqueux." C. R. Acad. Sci. Paris Series A-B, 152, pp. 1735-1739 (1911).

5 J. Boussinesq, "Sur la résistance qu'oppose un liquide indéfini en repos, sans pesanteur, au mouvement varié d'une sphère solide qu'il mouille sur toute sa surface, quand les vitesses restent bien continues et assez faibles pour que leurs carrés et produits soient négligeables" C. R. Acad. Sci. Paris, 100, pp. 935-937 (1885) (as cited in F. Mainardi and P. Pironi, Extracta Mathematica, 11, pp. 140-154.)

6 A.B. Basset, "On the motion of a sphere in a viscous liquid." *Phil. Trans. R. Soc. Lond.* A 179, pp. 43-63 (1888). (Also in A treatise on hydrodynamics, Chap. 22. Dover, 1961.)

7 E.E. Michaelides, "A novel way of computing the Basset term in unsteady multiphase flow computations." *Phys. Fluids*, 44, pp. 1579-1582 (1992).

8 J. Feng, and D.D. Joseph "The unsteady motion of solid bodies in creeping flows." *J. Fluid. Mech.* 303, pp. 83-102 (1995).

9 C.W. Oseen, "Uber die Stokes'sche formel, und uber eine verwandte Aufgabe in der Hydrodynamik." *Hydromechanik.*, 82, pp. 21-29 (1927).

10 T. Boggio, "Integrazione dell'equazione funzionale che regge la caduta di una sfera in un liquido viscoso." Atti. Accad. Naz. Lincei, 16, pp. 730-737 (1927).

for the nonexistence of other solutions is that there was no formulation of the particle momentum equation for a generic flow field that is not quiescent.

Tchen (1947)[11] dealt with the problem of modifying the particle equation of motion for the case of a uniform but time-dependent, free-stream flow field (the free-stream flow field is also called 'background' or 'unperturbed' flow field in this work.). The resulting equation, valid for the limit of infinitesimal particle Reynolds number (Re_p) and for uniform unsteady background flows, relates the transient acceleration of the particle with the time-dependent free-stream or background flow velocity. This equation is called in this work: Tchen's first equation of motion.

The common practice to overcome the lack of an analytical solution of Tchen's first equation is to neglect the troublesome history term and solve the simplified equation either by numerical or analytical methods. This practice has its roots in the fact that for particles of considerable size, the convective terms become important, and the drag force presents a nonlinear dependence on the relative velocity. This nonlinear dependence is accurately correlated for the steady-state drag, but is unknown for the unsteady term (for current efforts in modifying the kernel of the history term to include convective effects. The interested reader is referred to Mei and Adrian, 1991[12] and Kim et al, 1998)[13]. Because there is no analytically-derived equation describing the motion of a particle at high particle Reynolds number, there seemed to be little justification for considering the unsteady drag term. In fact, most current calculations use empirical coefficients for the steady-state drag coefficient and neglect completely the evolving profile around the particle, even though the higher Re_p number correction for the steady-state drag coefficient is not related to the evolving profile, but only to convective effects.

On the analytical side, attention was shifted to two new problems. These two problems were the correct derivation of the momentum equation for small particles in a non-uniform flow, and the calculation of the drag force form for small, non-spherical ellipsoids (Happel and Brenner, 1975[14]; Lawrence and Weinbaum, 1988[15]; Feng and Joseph, 1995)[16]. The analytical attempts to extend the Stokes limit to higher Reynolds numbers met little success (Oseen, 1927[17]), and no analytical expression for the momentum equation of particles moving at high particle Reynolds' number in unsteady flows is known to be accurate. Recently, Kim *et al.* (1998)[2] numerically

---

[11] C.M. Tchen "Mean value and correlation problems connected with the motion of small particles suspended in a turbulent fluid". Ph.D Thesis, Delft University 1947.

[12] R. Mei, R.J. Adrian, and J. Hanratty "Particle dispersion in isotropic turbulence under Stokes drag and Basset force with gravitational settling" *J. Fluid Mech.* 225, pp. 481-495 (1991).

[13] I. Kim, S. Elghobashi, and W.A. Sirignano, "On the equation for spherical particle motion: effects of Reynolds and acceleration numbers." *J. Fluid. Mech.*, 367, pp. 221-253 (1998).

[14] J. Happel, and H. Brenner, "Low Reynolds number hydrodynamics", Prentice-Hall, Englewood Cliffs, NJ (1975).

[15] C.J. Lawrence, and S. Weinbaum "The unsteady force on a body at low Reynolds number; the axisymmetric motion of a spheroid." *J. Fluid Mech.*, 189, pp. 463-489 (1988).

[16] J. Feng, and D.D. Joseph "The unsteady motion of solid bodies in creeping flows." *J. Fluid. Mech.* 303, pp. 83-102 (1995).

[17] C.W. Oseen, "Uber die Stokes'sche formel, und uber eine verwandte Aufgabe in der Hydrodynamik." Hydromechanik., 82, pp. 21-29 (1927).

simulated the convective flow around a heavy solid particle by solving the Navier-Stokes equations and modified the kernel of the history term for the range $1 < Re_p < 75$.

The first relevant work on the derivation of a particle equation of motion valid in non-uniform flows is also due to Tchen (1947)[11], who included an extra term relating the Laplacian of the undisturbed flow velocity to account for the effect of velocity gradients on the particle acceleration. Corrsin and Lumley (1956)[18] studied Tchen's work and modified the equation proposed by Tchen to account properly for the role of the pressure gradient on the force exerted by the fluid on the particle. The resulting expression derived by Corrsin and Lumley was still incomplete, mainly because it did not consider the second-order effects of the Laplacian of the fluid velocity on the steady and unsteady drag terms (the so-called Faxén corrections). Although these corrections are almost always small, the Faxén terms were not included in a consistent manner in Corrsin and Lumley's equation. Soo (1975)[19] and Gitterman and Steinberg (1980)[20] also suggested modifications on Tchen's equation, and there's still some controversy about the importance and consistency of both the total derivative term in the momentum equation and the correct form of the Faxén corrections (Auton *et al.*, 1988[21]). Maxey and Riley (1983)[22] derived a consistent equation of motion for a small particle in non-uniform flows. Some additional modifications of this equation for non-solid particles have been suggested in recent years (Auton *et al.*, 1988[21]; Mei *et al.*, 1991)[12].

The works cited in the previous paragraph were corrections and clarifications on the extension made by Tchen (1947)[11] in his second equation, which attempted to account for non-uniformity of the background flow field. Two modifications from the equation for uniform background flows are necessary. One is the inclusion of the Faxén corrections and the other is the modification of the forcing term, which is the term involving the substantial derivative of the fluid velocity at the particle position. It should be noted, however, that the Faxén correction terms are, in most cases, negligible since the equation of motion itself is only valid for small values of Re_p. The low particle Reynolds limit is generally accomplished only when very small particles are considered. The Faxén terms are important only when relevant velocity gradients on the scale of the particle velocity frequency are present in the background flow. The other modification of Tchen's first equation to accommodate non-uniform background flows was more important and much more damaging from the point of view of finding a general solution. In non-uniform background flows, the equation becomes nonlinear due to the need for knowing the velocity of the background flow field at the yet unknown current position of the particle.

Some conclusions can be drawn from looking back at these previous works concerned with the derivation of a particle's momentum equation for unsteady flows. First, the unsteadiness of the

---

18 S. Corrsin, and J. Lumley, "On the equation of motion for a particle in turbulent fluid." *Appl. Sci. Res.*, 6, pp. 114-116 (1956).

19 S.L. Soo, "Fluid dynamics of multiphase systems" Blaisdell, Waltham, MA (1975).

20 M. Gitterman and V. Steinberg, "Memory effects in the motion of a suspended particle in a turbulent fluid" *Phys. Fluids*, 23, pp. 2154-2167 (1980).

21 T.R. Auton, J.C.R. Hunt, and M. Proud'Homme, "The force exerted on a body in inviscid unsteady non-uniform rotational flow." *J. Fluid. Mech.*, 183, pp. 199-218 (1988).

22 M.R. Maxey and J.J. Riley, "Equation of motion for a small rigid sphere in a nonuniform flow" *Phys. Fluids*, 26, pp. 883-888 (1983).

evolving flow field around the particle adds great complexity to the description of the velocity history of the particle, so it is important to determine exactly when the history effects are important and when they can be neglected. Secondly, the only term that is significantly affected by the consideration of non-uniform flows is the time derivative of the background flow velocity, which becomes a substantial derivative of the flow velocity at the position of the particle. The substantial derivative makes the equation non-linear; however, one expects the relationship between the steady-state and the history drag terms not to be greatly affected by this modification, so that conclusions about the relative importance of individual terms in the equation drawn from the study of uniform flows can be extrapolated to non-uniform flows. Thirdly, the attempts to derive an equation valid in non-uniform flows diverted attention from Tchen's first equation of motion, so that this equation was never solved analytically for a generic and uniform background flow until the recent work of Coimbra and Rangel (1998)[23].

The third conclusion of the previous paragraph is of great relevance, since Tchen's first equation has all the terms of the Maxey-Riley equation, with the exception of the non-linear substantial derivative and the generally small Faxén corrections. The term represented by the substantial derivative in the Maxey-Riley equation is reduced in Tchen's equation to a time derivative of the fluid velocity (and valid for uniform or linear background flows).

Recall that the only known analytical solution for the particle velocity including the history drag is the one derived by Boggio (1927)[10]. The procedure used by Boggio, and then repeated by Sy, *et al.* (1970)[24] was to solve the equation of motion in Laplace space, and then invert back the final solution to time-space. The derivation is somewhat involved, and has led to mistakes. Perhaps because the solution of the integro-differential equation with constant forcing (the gravity acceleration term) was complicated, no successful attempts to solve the equation with a time-dependent forcing term were carried out.

Konopliv (1971)[25], in a short note that was more concerned with the analogy of the momentum and heat transfer equations, Laplace-transformed the first order integro-differential equation of motion for a quiescent case into a second-order differential equation. It appears that Konopliv did not realize that the resulting equation of motion was solvable by analytical methods. In fact, Konopliv suggested that the equation be solved by standard numerical methods with the aid of a 'digital computer'. If Konopliv had solved the equation derived in his note, he would have arrived at the same solution as did Boggio (1927)[10].

The procedure used by Konopliv (1971)[25] is of importance because, through the Laplace-transformation of the equation of motion, the history integral term can be singled out and transformed into a non-homogeneous term in a higher order differential equation. The resulting equation is of a higher order, but it becomes an ordinary differential equation rather than an integro-differential equation. Michaelides (1992)[7] followed the same procedure, but considered the more involved, time-dependent forcing term, instead of the equation with constant forcing

---

[23] C.F.M. Coimbra and R.H. Rangel, "General Solution of the Particle Equation of Motion in Unsteady Stokes Flows." *J. Fluid. Mech.*, 370, pp. 53-72 (1998).

[24] F. Sy, J.W. Taunton, and E.N. Lightfoot, "Transient creeping flow around spheres." *AIChE Journal* 16, pp. 386-391 (1970).

[25] N. Konopliv, "Gravitationally induced acceleration of spheres in creeping flow - a heat transfer analogy." *AIChE Journal*, 17, pp. 1502-1503 (1971).

considered by Konopliv. Michaelides developed a lengthy Laplace-transformation of Tchen's first equation, arriving at a second-order, ordinary differential equation for the relative velocity between the particle and the background flow velocity. Perhaps because of its complex appearance, or maybe because of the earlier suggestion made by Konopliv (1971)[25], Michaelides also did not solve his equation analytically. In fact, neither Michaelides nor Konopliv mention the fact that the resulting second-order differential equation is linear. Konopliv did not solve the second-order equation with constant forcing, and Michaelides used a standard Runge-Kutta method to solve the equation with unsteady forcing for both the gravitationally-induced motion and for a sinusoidally oscillating flow.

Coimbra and Rangel (1998)[23] applied a multiple-time-scale, fractional-differential linear operator to the equation derived by Tchen (1947),[11] transforming it into a second-order ODE (Ordinary Differential Equation) and then, using a variation of parameters, solved exactly the equation of motion for a small particle in unsteady Stokes flows. The solution presented by Coimbra and Rangel was derived in detail for an initial condition of zero relative velocity between the particle and the fluid. The general solution for an arbitrary initial velocity is shown in this report as a simple extension of the Heavy-side problem treated in the original paper (Coimbra and Rangel, 1998)[23]. The generalization of the solution for this case is important because it shows that the more involved equation derived by Michaelides through Laplace-transformation of the original integro-differential equation and the generic initial condition is not necessary. It suffices to derive the solution of the equation for zero initial velocity and then superimpose the particular solution to the Heavy-side problem for a given non-zero initial velocity. The solution for a generic Heavy-side problem is given in Coimbra and Rangel (1998)[23].

Lovalenti and Brady (1993)[26] and Galindo and Gerberth (1993)[27] derived an expression for the force acting on a droplet with internal recirculation under unsteady background flow conditions. Their equation is reduced to the one derived by Kim and Karila (1991)[28], if the viscosity of the droplet fluid is equal to the viscosity of the surrounding fluid. As with all the previously mentioned publications, with the exception of the monograph of Boggio (1927)[10] and the paper by Sy *et al.*, (1978)[24], these papers are concerned only with the derivation of the governing equations, and not with their solutions. The particle momentum equation is written implicitly with many terms involving the relative velocity and its derivatives, and a numerical solution of the momentum equation to determine the motion of the particle is suggested. Morrison and Stewart (1976)[29] studied the forces on a light, rigid sphere with perfect slip condition at its surface. The same problem, but with a generic slip boundary condition, was discussed by Michaelides and Feng (1995)[7,8].

---

[26] P.M. Lovalenti and J.F. Brady, "The hydrodynamic force on a rigid particle undergoing arbitrary time-dependent motion at small Reynolds number." *J. Fluid. Mech.* 256, pp. 342-356 (1993).

[27] V. Galindo and G. Gerberth, "A note on the force on an accelerating spherical drop at low Reynolds numbers." *Phys. Fluids*, 5, pp. 3290-3292 (1993).

[28] S. Kim and S.J. Karilla, "Micro hydrodynamics: Principles and Selected Applications", Butterworth-Heinemann. Boston, MA (1992).

[29] F.A. Morrison and M.B. Stewart, "Small bubble motion in an accelerating fluid." *J. Applied Mech.*, 97, pp. 399-402 (1976).

Because of the implication to turbulent flows, many authors have focused their attention to the particle motion in harmonic Stokes flows. Landau and Lifshitz (1959, 1987) determined the total drag acting on a small particle that moves harmonically through a quiescent fluid. This problem has important physical implications since it represents one of the simplest particle motions for which the history or Basset drag does not asymptote to zero for long times. The derivation presented in the work of Landau and Lifshitz focuses on the drag force for a particle that is moving harmonically in time. The relative velocity between the particle and the far-field flow in this case is exactly described by a sinusoidal function, since the background flow is quiescent. Other authors have since analyzed a more realistic case where the background fluid velocity is sinusoidal in time, and the particle is allowed to move under the forces acting on it. This is the problem under study in the present work. Virtual mass effects are included in the analysis as well as the Stokes and history drag forces. We will show that an analytical solution for the velocity of the particle can be found including initial transient effects. Previous works focusing on the harmonic motion of a single particle dealt with the stationary motion (Tchen, 1947[11]; Hjelmfelt and Mockros, 1966[30]; Morrison and Stuart, 1976[29]) which considers the long-term solution only, neglecting the initial transient.

Tchen (1947)[11] presented a solution of his equation of motion for the stationary case, and using Fourier analysis (and not the stationary solution) studied the influence of the Basset or History term in the motion of the particle. Hinze (1959) followed a similar procedure, but assumed both velocities of the particle and of the fluid as being passive of representation by Fourier integrals. This procedure allows us to calculate approximate amplitude ratios (neglecting a phase difference) and phase angles between the particle and the fluid. The procedure used by Hinze is essentially repeated in the work of Hjelmfelt and Mockros (1966)[30], where a more thorough study of the influence of individual terms in the equation of motion is presented. Chao (1968)[31] used yet another method to study the equation of motion. In his analysis, Chao Fourier-transformed Tchen's first equation of motion for the stationary case and derived the form of the Lagrangian auto-correlation coefficient. The ratio of particle-to-fluid "diffusivity" found through Chao's analysis is identical to the one found originally by Tchen. Chao also compared his results with more trivial results found by Soo (who neglected the pressure gradient effect, virtual mass and history drag forces) and Friedlander[32] (who neglected the virtual mass and history drag forces in his analysis).

Several forms of the equation of motion for a small particle moving in an unsteady flow have been studied in this century (Oseen, 1927[9]; Tchen, 1947[11]; Corrsin and Lumley, 1956[18]; and Maxey and Riley, 1983[22]), but few attempts have been made to solve the equation of motion for the velocity of the particle. Also, and most surprisingly, no previous attempts to describe generally the velocity of the particle as a function of the background flow characteristics have been conducted. The basic form of the equation of motion in uniform, unsteady flows has been

---

30 A.T. Hjelmfelt and L.F. Mockros, "Motion of Discrete Particles in a Turbulent Fluid" *Appl. Sci. Res.*, 16, pp. 149-161 (1966).

31 B.T. Chao, "Turbulent Transport Behavior of Small Particles in Dilute Suspension" Ósterreichisches Ingenieur-Archiv, 18, pp. 7-21 (1968).

32 S.K. Friedlander, "Behavior of Suspended Particles in a Turbulent Fluid" *AIChE Journal*, 3, pp. 381-388 (1957).

known for more than a century, but the so-called *Tchen's first equation* was never analytically solved in a general form.

The equation of motion for a small spherical particle moving in a uniform background flow field was originally derived by Tchen (1947)[11] and has been more recently extended to non-uniform background flow fields (Maxey and Riley, 1983[22]; Maxey, 1987). In terms of the relative velocity $\mathbf{w} = \mathbf{v} - \mathbf{u}$, where $\mathbf{v}$ and $\mathbf{u}$ are the particle and the fluid velocity respectively, the equation of motion is written as:

$$\frac{d\mathbf{w}}{d\hat{t}} + k\mathbf{w} + \sqrt{\frac{9\alpha}{2}}\,k\left\{\frac{1}{\sqrt{\pi}}\int_0^{\hat{t}}\frac{d\mathbf{w}}{d\sigma}\frac{d\sigma}{\sqrt{\hat{t}-\sigma}}\right\} = \mathbf{G}k - (1-\alpha)k\frac{d\mathbf{u}}{d\hat{t}}, \qquad (1)$$

where α is the fluid-to-particle density ratio, k is a virtual mass coefficient defined as $2/(2+\alpha)$, and $\mathbf{G}$ is a gravitational coefficient vector defined as $\mathbf{G} = (1-\alpha)\,\tau_p\,\mathbf{g}/U_o$. Velocities are made dimensionless by the flow characteristic velocity U_o. Time is made dimensionless by defining a particle characteristic time τ_p given by $2\tilde{n}_p a^2/9\grave{i}$. The vector g is the gravity acceleration, a is the radius of the spherical particle, ρ_p is the specific mass of the particle, and μ is the dynamic viscosity of the fluid.

The linear, integro-differential **Eq. (1)** can be transformed into a second-order non-homogeneous linear ODE with constant coefficients (Coimbra and Rangel, 1998[23]). The second-order equation can be solved exactly by the method of variation of parameters. The mathematical nature of the general solution depends on the sign of the discriminant of the characteristic equation associated with the homogeneous part of the second-order equation. The critical fluid-to-particle density ratio for which the mathematical nature of the solution changes character is α_c=8/5. The general solution of the particle equation of motion for values of α larger than α_c is:

$$\begin{aligned}
\mathbf{w}(\hat{t}) = &\left[1 + \sqrt{\frac{9\alpha}{2\Delta}}\,k^2\left(\frac{e^{R\hat{t}}\,erfc\left(\sqrt{R\,\hat{t}}\right)}{\sqrt{R}} - \frac{e^{Q\hat{t}}\,erfc\left(\sqrt{Q\,\hat{t}}\right)}{\sqrt{Q}}\right)\right]\mathbf{G} \\
&+ (1-\alpha)\frac{\left(e^{Q\hat{t}} - e^{R\hat{t}}\right)}{\sqrt{\Delta}}\,k\,\dot{\mathbf{u}}(0) \\
&+ (1-\alpha)\sqrt{\frac{9\alpha}{2\Delta}}\,k^2\left(\frac{e^{R\hat{t}}\,erf\left(\sqrt{R\,\hat{t}}\right)}{\sqrt{R}} - \frac{e^{Q\hat{t}}\,erf\left(\sqrt{Q\,\hat{t}}\right)}{\sqrt{Q}}\right)\dot{\mathbf{u}}(0) \\
&+ \frac{(1-\alpha)k\,e^{R\hat{t}}}{\sqrt{\Delta}}\int_0^{\hat{t}}\left[e^{-R\tau}\left(\sqrt{\frac{9\alpha}{2\pi}}\;k\int_0^{\tau}\frac{\ddot{\mathbf{u}}(\sigma)\,d\sigma}{\sqrt{\tau-\sigma}} - \ddot{\mathbf{u}} - k\,\dot{\mathbf{u}}\right)\right]d\tau \\
&- \frac{(1-\alpha)k\,e^{Q\hat{t}}}{\sqrt{\Delta}}\int_0^{\hat{t}}\left[e^{-Q\tau}\left(\sqrt{\frac{9\alpha}{2\pi}}\;k\int_0^{\tau}\frac{\ddot{\mathbf{u}}(\sigma)d\sigma}{\sqrt{\tau-\sigma}} - \ddot{\mathbf{u}} - k\,\dot{\mathbf{u}}\right)\right]d\tau,
\end{aligned} \qquad (2)$$

and for α smaller than α_c is:

$$\mathbf{w}(\hat{t}) = \mathbf{G} + \frac{2e^{-b\hat{t}/2}}{\sqrt{|\Delta|}}\left[\mathbf{G} - (1-\alpha)\dot{\mathbf{u}}(0)\right] k \sin\left(\frac{\sqrt{|\Delta|}\,\hat{t}}{2}\right)$$

$$- e^{-b\hat{t}/2}\left[\cos\left(\frac{\sqrt{|\Delta|}\hat{t}}{2}\right) + \frac{b}{\sqrt{|\Delta|}}\sin\left(\frac{\sqrt{|\Delta|}\hat{t}}{2}\right)\right]\mathbf{G}$$

$$+ \frac{2e^{-b\hat{t}/2}}{\sqrt{|\Delta|}}\sin\left(\frac{\sqrt{|\Delta|}\hat{t}}{2}\right)\left\{\sqrt{\frac{9\alpha}{2\pi}}k^2\left[(1-\alpha)\dot{\mathbf{u}}(0) - \mathbf{G}\right]\int_0^{\hat{t}}\frac{e^{b\tau/2}}{\sqrt{\tau}}\cos\left(\frac{\sqrt{|\Delta|}\tau}{2}\right)d\tau\right.$$

$$\left. + \int_0^{\hat{t}} e^{b\tau/2}\cos\left(\frac{\sqrt{|\Delta|}\tau}{2}\right)(1-\alpha)\left(\sqrt{\frac{9\alpha}{2\pi}}k^2\int_0^{\tau}\frac{\ddot{\mathbf{u}}(\sigma)d\sigma}{\sqrt{\tau-\sigma}} - k\,\ddot{\mathbf{u}} - k^2\,\dot{\mathbf{u}}\right)d\tau\right\}$$

$$- \frac{2e^{-b\hat{t}/2}}{\sqrt{|\Delta|}}\cos\left(\frac{\sqrt{|\Delta|}\hat{t}}{2}\right)\left\{\sqrt{\frac{9\alpha}{2\pi}}k^2\left[(1-\alpha)\dot{\mathbf{u}}(0) - \mathbf{G}\right]\int_0^{\hat{t}}\frac{e^{b\tau/2}}{\sqrt{\tau}}\sin\left(\frac{\sqrt{|\Delta|}\tau}{2}\right)d\tau\right.$$

$$\left. + \int_0^{\hat{t}} e^{b\tau/2}\sin\left(\frac{\sqrt{|\Delta|}\tau}{2}\right)(1-\alpha)\left(\sqrt{\frac{9\alpha}{2\pi}}k^2\int_0^{\tau}\frac{\ddot{\mathbf{u}}(\sigma)d\sigma}{\sqrt{\tau-\sigma}} - k\,\ddot{\mathbf{u}} - k^2\,\dot{\mathbf{u}}\right)d\tau\right\}. \tag{3}$$

In **Eqs. (2)** and **(3),** the particle is assumed to be in dynamical equilibrium with the background flow at $\hat{t}=0$, so that $\mathbf{w}(0)=0$. The dots denote integer derivatives with respect to $\hat{t}$ or with respect to the dummy variables of integration σ or τ. The following coefficients are used in **Eqs. (2)** and **(3)** to simplify the notation: $b=(2k-9\alpha k^2/2)$, $\Delta=b^2-4k^2$, $Q=(-b-\sqrt{\Delta})/2$, and $R=(-b+\sqrt{\Delta})/2$. The general solutions of the equation of motion, **Eqs. (2)** and **(3),** are particularized to harmonic Stokes flows in the next section, and the exact solution is compared to the solution found when history effects are neglected. The comparison shows that history effects are indeed more pronounced in the critical frequency range $(\Omega \approx 9\nu/a^2)$ and negligible elsewhere.

CURRENT RESEARCH

Theory

Summary

During the theoretical effort, we developed a procedure to solve the equation exactly (to the approximations made in the derivation of the equation) for a generic, uniform flow field $\mathbf{U}(t)\neq 0$.

This was accomplished by applying a fractional differential operator to a dimensionless form of the particle equation of motion. This procedure yields a second-order, explicit, differential equation in the relative particle-to-fluid velocity. During the derivation of the explicit equation,

attention is given to the identification of the terms in this equation with the original forces that generate them. The resulting linear, non-homogenous, second-order ordinary equation is then solved exactly using variation of parameters.

We have treated three specific cases using the general solutions derived in the last section. The first is the gravitationally-induced motion of a sphere in a quiescent fluid. The second case treated was the response of a particle undergoing an impulsive start. A similar problem treated in our work is the problem of a spherical particle that is initially stationary in a fluid that undergoes an impulsive start to a constant velocity. The time derivative of the background flow velocity in this case is a delta function acting at $t = 0^+$. The third case treated is concerned with the motion of a sphere that is allowed to move under the forces generated by a sinusoidal surrounding field. This case is presented in detail in the next section.

A scaling analysis on the forces that depend on the fluid-to-particle density ratio yielded the value of a critical forcing frequency for which the history term effects are maximum velocity in harmonic Stokes flows. The scaling analysis is validated against the exact analytical solution of the particle equation of motion for a harmonic background flow, as well as against the stationary analysis. The stationary analysis shows that differences between the predicted behavior with and without the history term are relevant in the range $0.1 < S < 10$, as predicted by the simplified scaling analysis. Depending on the forcing frequency, the forces acting on the particle can be dominated by either the steady-state Stokes drag (low frequencies) or by virtual mass effects (at high frequencies). When the forcing frequency is of the order of the critical frequency $9\nu/a^2$, all forces are of the same order of magnitude and must be considered. The comparison of the exact analytical solution of the equation of motion with the quasi-steady formulation confirmed the scaling analysis. The scaling analysis also showed that the displacement of the fluid oscillations must be of the order of the particle radius (or less) to comply with the small particle Reynolds number restriction. The critical frequency for maximum history effects depends directly on the kinematic viscosity of the fluid and inversely on the square of the radius of the particle. An error analysis was developed to study the effects of uncertainties in the measurements of viscosity and position displacements.

It is well known that the steady Stokes flow perturbation caused by the presence of a sphere propagates to a relatively large distance[33] This reference cites that for $r \sim 20\ a$, the velocities are still about 5% of the free-stream value: the r-velocity at $r \sim 10\ a$ is $\sim 7.5\%$ lower and the tangential θ-velocity at $r \sim 10$ is $\sim 4\%$ lower than their respective free-stream values. However, at higher frequencies, the friction force acting on the particle is controlled by the unsteadiness of the near field, and less influence from the free-stream condition is felt by the particle. Therefore, estimates based on the steady drag are conservative.

The theory also handles non-zero initial velocities. For $\alpha = 2$, the influence of a non-zero initial velocity decays quickly so that it becomes negligible for values of $t > 10\ \tau_p$. For the conditions in our experiment, this corresponds to approximately 27 ms. The influence of a non zero velocity in our experiments becomes negligible after the particle travels less than one radius of distance from the initial location. This is true even when the terminal velocity of the particle is used as the initial velocity difference.

---

[33] F.M. White (1991) Viscous Fluid Flow, McGraw-Hill.

Relative Scaling of the Virtual Mass, History and Stokes Drag Forces

Consider the motion of a particle subjected to a free-stream flow that oscillates sinusoidally in time. After the initial transient caused by the initial condition $\mathbf{w}(0) = 0$, the particle engages in a motion that can be approximately described by a sinusoidal wave. The relative velocity, **w,** is thus also a sinusoidal wave with the same frequency of the background fluid velocity but with amplitude **b** and a phase difference. The virtual mass, history and Stokes drag forces are thus given by:

$$\mathbf{f}_{VM} = \frac{\alpha}{2}\frac{d\mathbf{w}}{d\hat{t}} = \frac{\mathbf{b}\alpha}{2}\frac{d\left[\sin(\omega\hat{t})\right]}{d\hat{t}} = \frac{\mathbf{b}\alpha\omega\cos(\omega\hat{t})}{2} \cong O\left(\mathbf{b}\frac{\alpha\omega}{2}\right), \tag{4}$$

$$\mathbf{f}_{H} = H\sqrt{\pi}\frac{d^{1/2}\mathbf{w}}{d\hat{t}^{1/2}} = \mathbf{b}H\sqrt{\omega\pi}\frac{d^{1/2}\left[\sin(\omega\hat{t})\right]}{\left[d(\omega\hat{t})\right]^{1/2}} \cong O\left(\mathbf{b}\sqrt{\frac{9\alpha\omega}{2}}\right), \tag{5}$$

$$\mathbf{f}_{St} = \mathbf{w} = \mathbf{b}\sin(\omega\hat{t}) \cong O(\mathbf{b}), \tag{6}$$

Note that for the history drag force, the generalized chain rule for fractional derivatives was used. For $(x) = \omega x$, the generalized chain rule gives simply:

$$\frac{d^n f(\omega x)}{dx^n} = \omega^n \frac{d^n f(\omega x)}{[d(\omega x)]^n}. \tag{7}$$

The relative scaling of the three dimensionless forces is thus:

$$\left\langle |\mathbf{f}_{VM}| : |\mathbf{f}_{H}| : |\mathbf{f}_{St}| \right\rangle = \left\langle S : 3S^{1/2} : 1 \right\rangle, \tag{8}$$

where $S = \alpha\omega/2$. The maximum influence of the history drag occurs when:

$$\partial\left\{|\mathbf{f}_{H}| \Big/ \left(|\mathbf{f}_{VM}| + |\mathbf{f}_{H}| + |\mathbf{f}_{St}|\right)\right\}\Big/\partial S = 0,$$

which corresponds to $S = 1$ or $\alpha\omega = 2$. The scaling relation in **Eq. (8)** also shows that when $\alpha\omega = 2$ the amplitude of the history drag force is three times larger than the amplitude of the virtual mass and the Stokes drag forces. When the value of the product $\alpha\omega$ is much smaller than 2, the Stokes drag dominates. For values of $\alpha\omega$ much larger than 2, the virtual mass force is dominant. **Figure 1** shows graphically the scaling of the individual forces.

Note that the product $\alpha\omega$ does not depend on the density of the particle. The dimensionless number that governs the scaling of the forces is:

$$S = \frac{\alpha\omega}{2} = \frac{\Omega}{\nu}\left(\frac{a}{3}\right)^2, \tag{9}$$

where Ω is the dimensional forcing frequency and ν is the kinematic fluid viscosity.

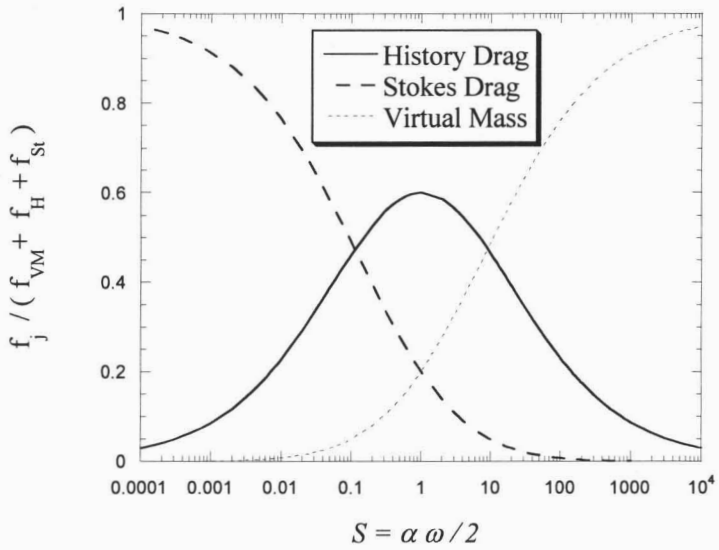

Figure 1. Relative scaling of the forces for harmonic particle motion.

It is important to emphasize that the preceding scaling analysis gives only a limited view of the actual behavior of the particles. This limitation is because only the relative scaling of the forces that depend on the velocity driving potential is determined by the analysis. The actual velocity response of the particle can be determined only from the solution of the equation of motion. The next section is dedicated to the particularization of the general solutions, **Eqs. (2)** and **(3),** to the case of harmonic Stokes flows.

Since S is an important parameter for this study, we offer the following additional discussion of its significance:

> *The parameter, S, is a dimensionless frequency of oscillation, normalized so that it has a value of 1 when the history drag effects are maximum. Physically, S is the ratio of the viscous time scale to the external oscillation time scale. The viscous time scale is the time required for information from the surface of the particle to reach a distance comparable to the size of the particle. When the two time scales are of the same order of magnitude, the unsteadiness of the near field becomes relevant and thus the history drag reaches its maximum.*
>
> *When S is much smaller than 1, steady viscous contributions become more relevant. The pressure field around the particle is also unsteady, and at very high values of S, this unsteadiness (the so-called virtual mass effect) is dominant and viscous effects are negligible. This is because at very high vibrational frequencies the only relevant force is the one caused by the pressure field, and the viscosity of the fluid is irrelevant since both Stokes and history drags become negligible.*
>
> *The special case of S=1 represents a condition where the whole field around the particle is relevant because there is no dominant effect either from the steady drag or from the pressure field. When the history term is important, all other forces are also important.*

Exact Solution of the Equation of Motion for Harmonic Stokes Flows

The general solutions of **Eqs. (2)** and **(3)** are particularized to a background fluid velocity $\mathbf{u} = \mathbf{a}\sin(\omega\hat{t})$, yielding for $\alpha > 8/5$:

$$\mathbf{w}(\hat{t}) = \frac{\mathbf{a}(1-\alpha)k\omega\, e^{Q\hat{t}}}{\sqrt{\Delta}}\left[1-\left(\frac{\omega^2 - Qk}{Q^2-\omega^2}\right)-\sqrt{\frac{9\alpha}{2Q}}\,k\,erf\left(\sqrt{Q\hat{t}}\right)\right]$$

$$-\frac{\mathbf{a}(1-\alpha)k\omega\, e^{R\hat{t}}}{\sqrt{\Delta}}\left[1-\left(\frac{\omega^2 - Rk}{R^2-\omega^2}\right)-\sqrt{\frac{9\alpha}{2R}}\,k\,erf\left(\sqrt{R\hat{t}}\right)\right]$$

$$+\frac{\mathbf{a}(1-\alpha)k\omega}{\sqrt{\Delta}}\left[\frac{(k+Q)\omega}{Q^2+\omega^2} - \frac{(k+R)\omega}{R^2+\omega^2}\right]\sin(\omega\hat{t})$$

$$+\frac{\mathbf{a}(1-\alpha)k\omega}{\sqrt{\Delta}}\left[\frac{Rk-\omega^2}{R^2+\omega^2} - \frac{Qk-\omega^2}{Q^2+\omega^2}\right]\cos(\omega\hat{t})$$

$$+\frac{\mathbf{a}(1-\alpha)k^2\omega^2}{\sqrt{\Delta}}\sqrt{\frac{9\alpha}{2\pi}}\left\{\begin{array}{l} e^{Q\hat{t}}\int_0^{\hat{t}}\left[e^{-Q\tau}\left(\int_0^{\tau}\frac{\sin(\omega\sigma)d\sigma}{\sqrt{\tau-\sigma}}\right)\right]d\tau \\ -e^{R\hat{t}}\int_0^{\hat{t}}\left[e^{-R\tau}\left(\int_0^{\tau}\frac{\sin(\omega\sigma)d\sigma}{\sqrt{\tau-\sigma}}\right)\right]d\tau \end{array}\right\}, \tag{10}$$

and for $\alpha < 8/5$:

$$\mathbf{w}(\hat{t}) = \frac{2\mathbf{a}\omega(1-\alpha)e^{-b\hat{t}/2}}{\sqrt{|\Delta|}}\sqrt{\frac{9\alpha}{2\pi}}k^2\left\{\begin{array}{l} \sin\left(\frac{\sqrt{|\Delta|}\hat{t}}{2}\right)\int_0^{\hat{t}}\frac{e^{b\tau/2}}{\sqrt{\tau}}\cos\left(\frac{\sqrt{|\Delta|}\tau}{2}\right)d\tau \\ -\cos\left(\frac{\sqrt{|\Delta|}\hat{t}}{2}\right)\int_0^{\hat{t}}\frac{e^{b\tau/2}}{\sqrt{\tau}}\sin\left(\frac{\sqrt{|\Delta|}\tau}{2}\right)d\tau \end{array}\right\}$$

$$+\frac{2\mathbf{a}\omega^2(1-\alpha)e^{-b\hat{t}/2}}{\sqrt{|\Delta|}}\sqrt{\frac{9\alpha}{2\pi}}k^2\left\{\begin{array}{l} \cos\left(\frac{\sqrt{|\Delta|}\hat{t}}{2}\right)\int_0^{\hat{t}}\left[e^{b\tau/2}\sin\left(\frac{\sqrt{|\Delta|}\tau}{2}\right)\int_0^{\tau}\frac{\sin(\omega\sigma)}{\sqrt{\tau-\sigma}}d\sigma\right]d\tau \\ -\sin\left(\frac{\sqrt{|\Delta|}\hat{t}}{2}\right)\int_0^{\hat{t}}\left[e^{b\tau/2}\cos\left(\frac{\sqrt{|\Delta|}\tau}{2}\right)\int_0^{\tau}\frac{\sin(\omega\sigma)}{\sqrt{\tau-\sigma}}d\sigma\right]d\tau \end{array}\right\}$$

$$+\frac{2\mathbf{a}\,\omega(1-\alpha)e^{-b\hat{t}/2}}{\sqrt{|\Delta|}}\left\{\begin{array}{l}\sin\left(\dfrac{\sqrt{|\Delta|}\hat{t}}{2}\right)\displaystyle\int_0^{\hat{t}} e^{b\tau/2}\cos\left(\dfrac{\sqrt{|\Delta|}\tau}{2}\right)\left[\omega\sin(\omega\tau)-k\cos(\omega\tau)\right]d\tau \\ -\cos\left(\dfrac{\sqrt{|\Delta|}\hat{t}}{2}\right)\displaystyle\int_0^{\hat{t}} e^{b\tau/2}\sin\left(\dfrac{\sqrt{|\Delta|}\tau}{2}\right)\left[\omega\sin(\omega\tau)-k\cos(\omega\tau)\right]d\tau\end{array}\right\}. \tag{11}$$

If the history term contribution is neglected, the solution of the simplified equation of motion is given simply by (the subscript '*nh*' stands for 'no history'):

$$\mathbf{w}_{nh}(\hat{t}) = \left(1-e^{-k\hat{t}}\right)\mathbf{G} - Pke^{-k\hat{t}}\int_0^{\hat{t}} e^{k\sigma}\dot{\mathbf{u}}(\sigma)d\sigma, \tag{12}$$

which gives for a sinusoidal background velocity:

$$\mathbf{w}_{nh}(\hat{t}) = \frac{\mathbf{a}\,\omega\,k(1-\alpha)}{k^2+\omega^2}\left[k\,e^{-k\hat{t}} - k\cos(\omega\hat{t}) - \omega\sin(\omega\hat{t})\right]. \tag{13}$$

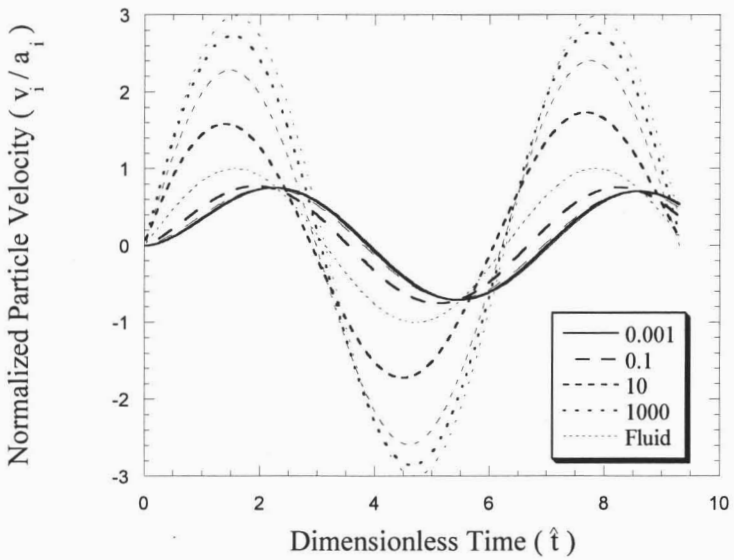

Figure 2. Normalized particle velocities for ω=1 and different values of α. The thick lines represent the full solutions, Eqs. (10) and (11), and the thin lines represent the solution neglecting history effects, Eq. (13).

Figure 2 and **Figure 3** show the increasing influence of the history term when the product $\alpha\omega$ approaches the value of 2 (this observation will be further discussed). Of particular interest is the fact that the absolute maximum of the relative velocity **w** is always smaller than the absolute maximum of its "*no-history*" counterpart $\mathbf{w}_{nh}$, although being of the same order of magnitude.

Figure 3 shows the particle velocity behavior given by solutions, **Eqs. (10), (11)** and **(13),** for different values of the fluid-to-particle-density ratio and dimensionless forcing frequencies. The range of values of the product $\alpha\omega$ covered in these figures is $[10^{-3}: 10^{5}]$, varying from the steady-state Stokes drag regime to the virtual mass force regime. The thick lines in all figures indicate the full solutions, **Eqs. (10)** and **(11).** The thin lines indicate the behavior given by the solution **Eq. (13).**

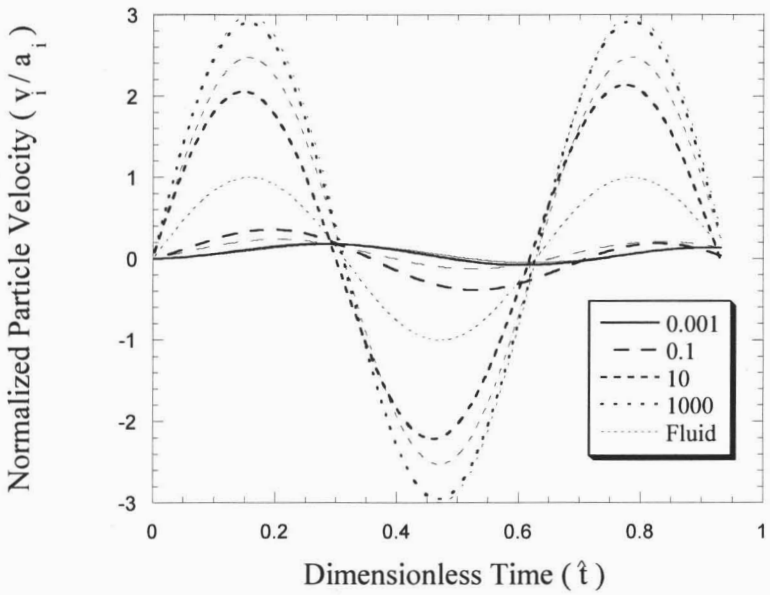

Figure 3. Same as Figure 2 but for $\omega = 10$.

After the initial exponential decay, the amplitude of the relative velocity $\mathbf{w}_{nh}$ is of order:

$$\omega|\alpha-1|k(k+\omega)/\left(k^2+\omega^2\right).$$

This observation is important to determine the magnitude of the displacement amplitude for which the history drag force becomes dominant. The constraint of small Re_p places a tight limit on the displacement amplitude for which it is possible to reach the range $S \sim 1$, where history effects are dominant.

The *particle Reynolds number* is first approximated as:

$$\mathrm{Re}_p \equiv \frac{a|\mathbf{V}-\mathbf{U}|}{\nu} = \frac{a\,\mathbf{A}\bullet\mathbf{w}}{\nu} \le \frac{a\,\mathbf{A}\bullet\mathbf{w}_{nh}}{\nu} \cong O\left\{\frac{\omega|\alpha-1|k(k+\omega)|\mathbf{A}|a}{\nu\left(k^2+\omega^2\right)}\right\}. \tag{14}$$

Equation (14) restricts the dimensional velocity amplitude of the background flow $|\mathbf{A}|$ to satisfy:

$$|\mathbf{A}| < \frac{\nu\left(k^2+\omega^2\right)}{\omega|\alpha-1|k(k+\omega)\,a}. \tag{15}$$

From **Eq. (15),** the dimensional frequency for $S = 1$ (maximum history effects) is:

$$\Omega_{S=1} = \nu\left(\frac{3}{a}\right)^2, \tag{16}$$

which, when combined with **Eq. (15)** and $\omega = 2/\alpha$, gives for the maximum amplitude of the background displacement:

$$\frac{|\mathbf{A}|}{\Omega} < \left(\frac{\alpha + (2+\alpha)^2/\alpha}{4|\alpha - 1|[1 + (2+\alpha)/\alpha]}\right) a = f(\alpha)\, a \tag{17}$$

The function $f(\alpha)$ in **Eq. (17)** is larger than 1 only when the density of the particle is very similar to the density of the fluid. Thus, in order to comply with the restriction on Re_p for particles with density differing from the density of the fluid, and to have significant history effects, the displacement amplitude of the background flow has to be of the order of the radius of the particle, or smaller. If the amplitude of the oscillations increase, the small Re_p restriction is not satisfied, and the convective terms in the Navier-Stokes equation cannot be neglected. Since higher-order approximations on Re_p predict lesser effects of the history term contribution with increasing Re_p (Lovalenti and Brady, 1993[26]), **Eq. (17)** gives an upper bound for the amplitude of displacement oscillations that are strongly affected by the history drag. In other words, history drag effects in harmonic flows are maximized when the forcing frequency approaches the value given by **Eq. (15)** and for displacement amplitudes smaller than the radius of the particle.

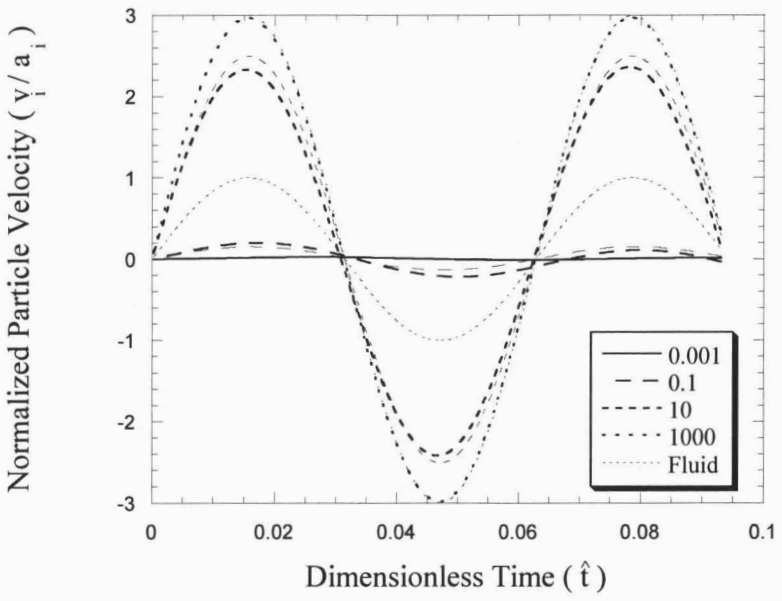

Figure 4. Same as Figure 3 but for $\omega = 100$.

Figure 5 and **Figure 6** show velocity and displacement plots, respectively, for a specific case of interest. This case corresponds to $\alpha\omega = 2$, where history effects are maximized. The dimensional frequency of the oscillation is equal to 57.3 Hz, and the particle density is equal to half the density of the surrounding fluid. The particle diameter is equal to 200 μm and the kinematic viscosity of the fluid is $\nu = 40\times10^{-6}$ m^2/s. This case was selected to test the

experimental equipment under Earth-gravity conditions. The gravity settling velocity of such a particle under the above conditions is roughly 2.5 cm/s.

Another interesting feature shown in **Figure 5** and **Figure 6** is the phase difference between the fluid velocity and the particle velocity. For particles heavier than the fluid, there is a phase lag caused by the inability of the particle to respond rapidly to fluid velocity variations due to its larger inertia. For the case of the light particles, the situation is reversed because of the combined effect of the history drag and virtual mass forces. The phase difference for light particles is negative because the relative acceleration is very important to determine the particle behavior. This becomes clear when it is observed that, for a light particle, the particle velocity always changes sign before the fluid velocity does. If the force on the particle were only a function of the relative velocity (as in the quasi-steady formulation), this behavior would not be predicted. The actual behavior of light particles shows how much the pressure and stress gradients due to the time derivatives of the relative velocity affect the forces on a particle with smaller inertia.

The fact that the light particles are heavily influenced by the time derivatives of the relative velocity is clearly understood if one thinks of a suspended bubble in a fluid moving with constant velocity. If the fluid is moving for a time much longer than the response time of the bubble (which, due to virtual mass effects, is better characterized as τ_p / k), the particle will move with zero relative velocity with respect to the fluid. To a fixed observer, the bubble is moving with the fluid velocity. Now, if the fluid acquires a constant negative acceleration, the bubble also starts accelerating in the negative direction. After a sufficient time, the bubble reaches its terminal velocity associated with the deceleration rate of the fluid. For the fixed observer, the bubble will be moving with the decreasing velocity of the fluid plus its terminal velocity. When the velocity of the fluid reaches a value equal to minus the terminal velocity of the bubble, the bubble is at rest for the fixed observer. The time for the fluid to reach zero velocity from that point on is a phase lag for the fluid–the bubble is already moving with respect to the fixed observer, but the fluid has not yet reached zero velocity. This simple example of linear acceleration shows the importance of the combined virtual mass and "acceleration" drag forces. The term "acceleration drag" was used to describe the history drag (Tchen, 1947[11]) but is not very adequate because of the half derivative dependence on the relative velocity that the history term presents, and not on the first derivative. The terminology is, however, interesting for emphasizing the dependence of bubble behavior on the acceleration of the fluid (or perhaps, on the "half-acceleration" also).

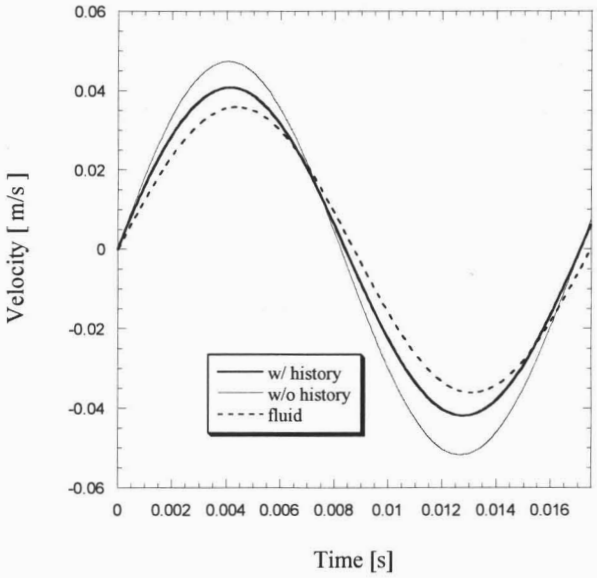

Figure 5. Velocity plots for the case $\alpha\omega = 2$.

In the particular case depicted in **Figure 5** (density of the fluid is twice as large as the density of the particle), the estimation of the particle Reynolds number made using **Eq. (14)** is slightly too conservative. **Figure 7** shows an upper bound of the particle Reynolds number for two different amplitude displacements of the fluid and for varying forcing frequencies as estimated by **Eq. (14).**

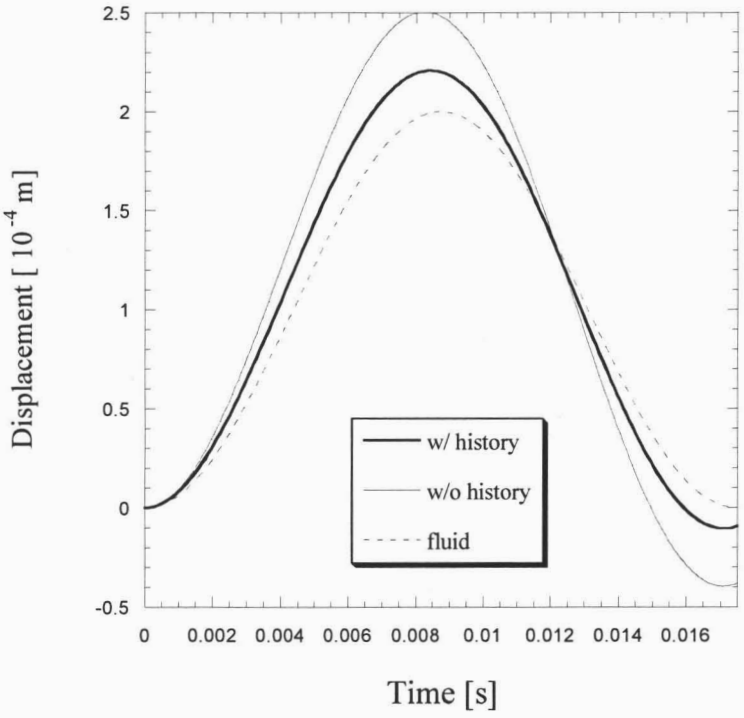

Figure 6. Displacement plots for the case $\alpha\omega = 2$.

The maximum particle Reynolds number for a forcing frequency equal to 57.3 Hz, a = 1 mm, $\nu = 40 \times 10^{-6}$ m^2/s, and a fluid displacement $\Delta x = 100$ μm is calculated as:

$$\mathrm{Re}_p = \frac{a\mathbf{W}}{\nu} \sim 0.15\,\frac{a\Delta x\Omega}{\nu} = 0.15\,\frac{1\times10^{-3}\,m \times 100\times10^{-6}\,m \times 360\,rad/s}{40\times10^{-6}\,m^2/s} = 0.135 \quad . \quad (18)$$

Figure 5 shows the maximum fluid-to-particle relative velocity as approximately 15% of the maximum fluid velocity). **Figure 7** gives for the same case a value of approximately 0.5, indicating that the estimation of the particle Reynolds number by **Eq. (14)** is a conservative one, as expected.

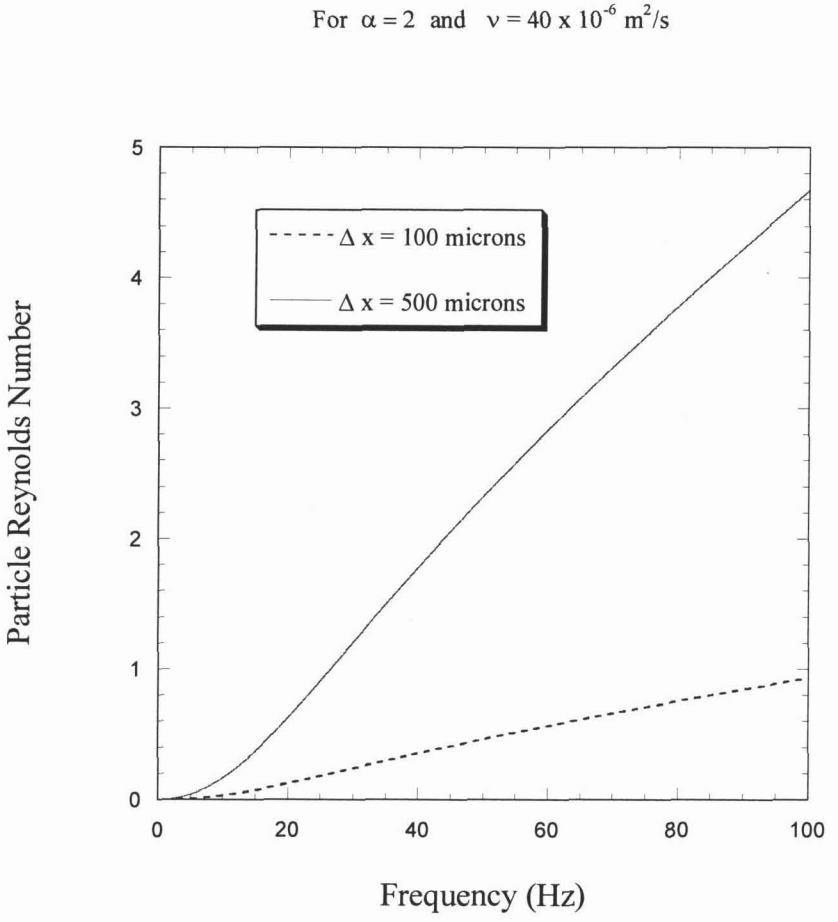

Figure 7. Estimated particle Reynolds number (Eq. (14)) *vs.* frequency.

Finally, in order to validate the scaling analysis presented in the last section, the behavior of the maximum amplitudes of **Eqs. (10)** and **(12)** are studied for different frequencies. This is graphically depicted in **Figure 8** for the same study case (a = 1 mm, $\nu = 40 \times 10^{-6}$ m^2/s, and $\alpha = 2$). **Figure 8** clearly shows the maximum history effects for a frequency f ~ 60 Hz, where $S \sim 1$.

For $\alpha = 2$, $d_p = 2$ mm, and $\nu = 40 \times 10^{-6}$ m^2 / s

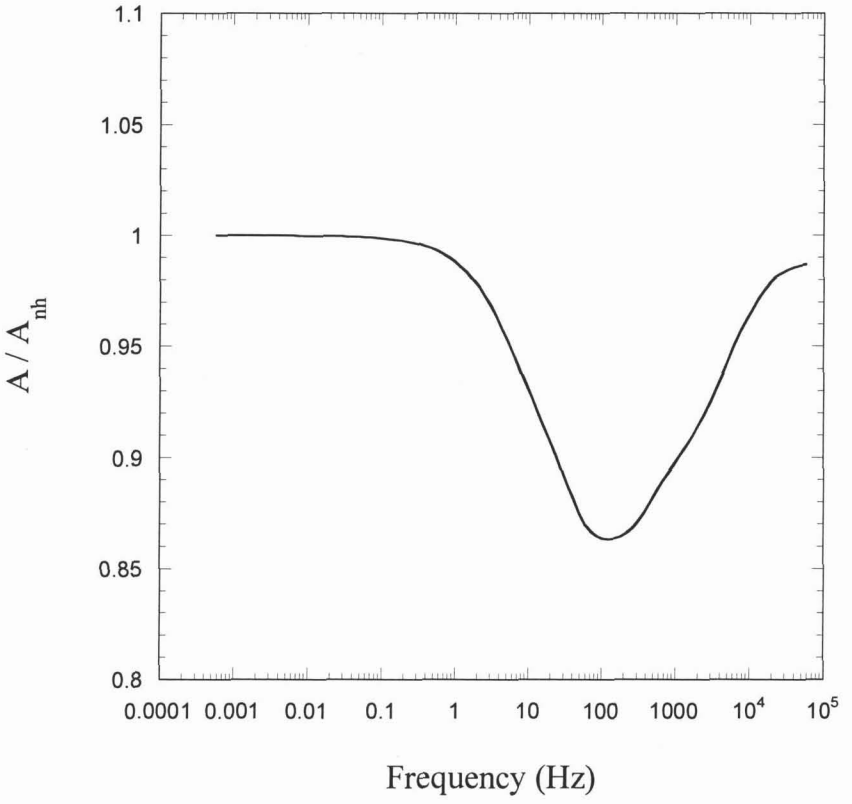

Figure 8. Influence of the history term in the velocity amplitude of the particle motion. The discrete points result from analytical evaluation of the particle behavior considering (or not) the history term. The continuous line is included to show the approximate behavior of the solutions. Note the maximum influence of the history term (minimum of the curve) when f ~ 60 Hz , $S \sim 1$.

Stationary Analysis

The stationary analysis, that is, the solution of **Eq. (1),** neglecting the initial transients, has been studied by several authors in the past (Tchen, 1947[11]; Hinze, 1959; Hjelmfelt and Mockros, 1966[30]; Chao, 1968[31]; Morrison and Stewart, 1976[29]). Although the specifics of the techniques have been used by the previous authors, the basic idea is the same: the velocity of the particle and the velocity of the background fluid are expressed as Fourier integrals of the form:

$$u_i = \int_0^\infty \left(\zeta \cos\omega\hat{t} + \lambda \sin\omega\hat{t}\right) d\omega \quad , \tag{19}$$

$$v_i = \int_0^\infty \left(\chi \cos\omega\hat{t} + \varphi \sin\omega\hat{t}\right) d\omega \quad . \tag{20}$$

The velocities given by **Eqs. (19)** and **(20)** are then forced to satisfy **Eq. (1),** and the velocity of the particle is then expressed as:

$$v_i = \int_0^\infty \eta\left(\zeta \cos\left(\omega \hat{t} + \phi\right) + \lambda \sin\left(\omega \hat{t} + \phi\right)\right) d\omega \quad , \tag{21}$$

where:

$$\eta = \sqrt{(1+g_1)^2 + g_2^2} \quad , \tag{22}$$

and:

$$\phi = \tan^{-1}\left(\frac{g_2}{1+g_1}\right) . \tag{23}$$

The two auxiliary functions $g_1(S,\alpha)$ and $g_2(S,\alpha)$ are calculated from the algebraic substitution of Eq. (19) and Eq. (20) into Eq. (1).

Figure 9 and **Figure 10** show the amplitude ratio $\eta\,(1 + b_i / a_i)$ and the phase difference ϕ as a function of the scaling number *S*.

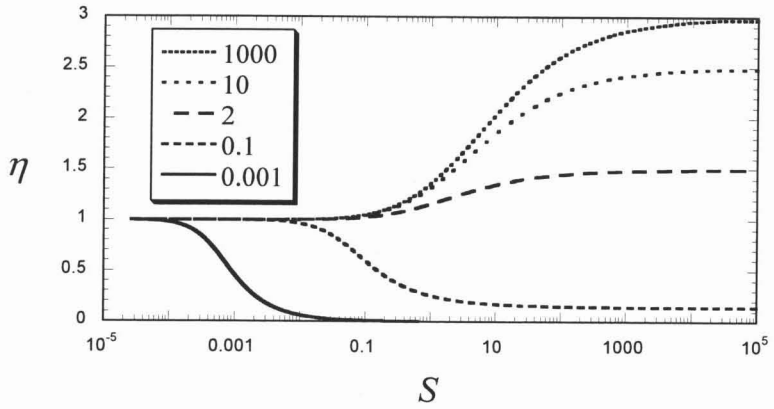

Figure 9. Amplitude ratio for different values of α.

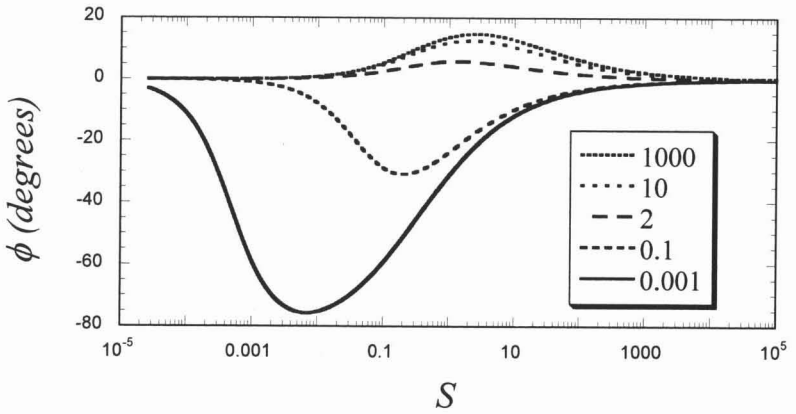

Figure 10. Phase difference for different values of α.

The maximum phase difference for the case being studied ($\alpha = 2$) is 5.85 degrees, which occurs for $S = 1.41$ ($f \sim 85$ Hz in 40 centistokes' Krytox and $a = 1$ mm). For $S = 1$ ($f \sim 60$ Hz, same as conditions above) the phase advance of the light particle in question is only 5.78 degrees. The amplitude ratio for $S = 1$ is equal to 1.16 when history effects are considered. This amplitude ratio is 1.30 when history effects are neglected.

The small expected values for the phase difference in the selected case make the simplified scaling analysis for the ratio of the forces accurate (see **Figure 5**). Note that negative phase differences above mean delay (heavy particles). Conversely, positive phase differences mean advance (light particles).

It can also be inferred from **Figure 9** and **Figure 10** that, for the case in study, and for $S > 3$, the phase difference is negligible and the amplitude ratio approaches the asymptotic value of 1.50. Since one of the objectives of the ground experiment is to validate the theoretical analysis for the selected case, this case is depicted in detail in **Figure 9** and **Figure 10**. Note the significant difference in phase advance obtained when history effects are taken into account. Analog curves for the other cases in the test matrix are shown in **Figure 11.**

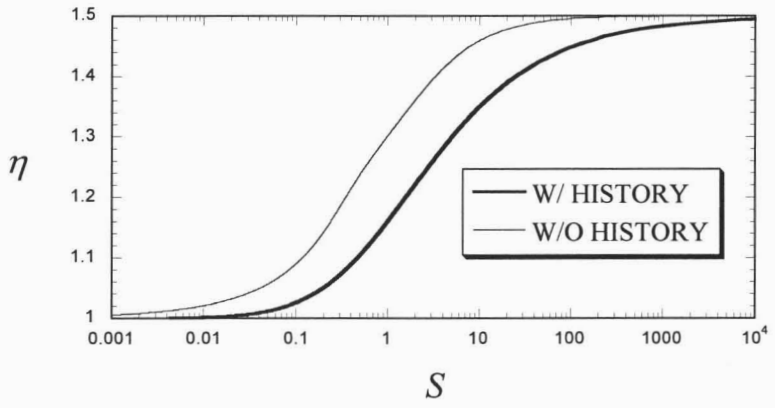

Figure 11. Amplitude ratio for α = 2.

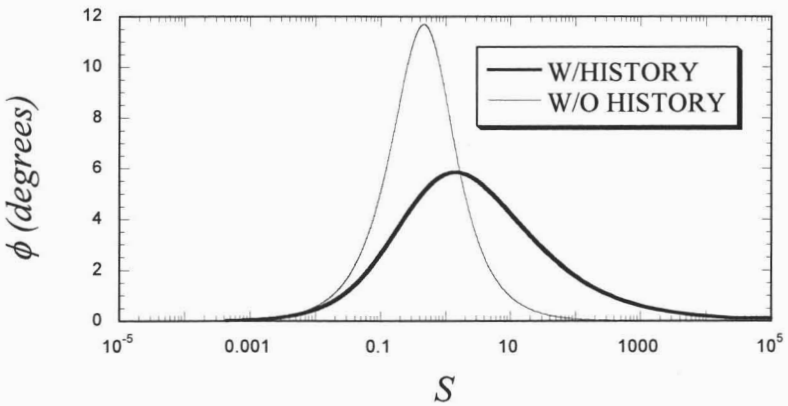

Figure 12. Phase difference for α = 2.

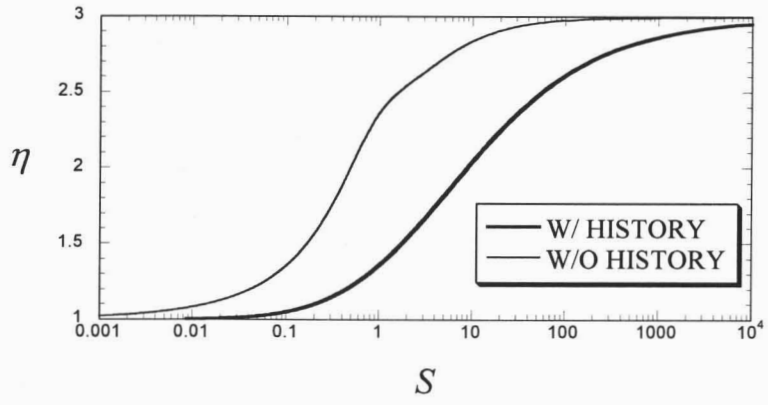

Figure 13. Amplitude ratio for α = 1000.

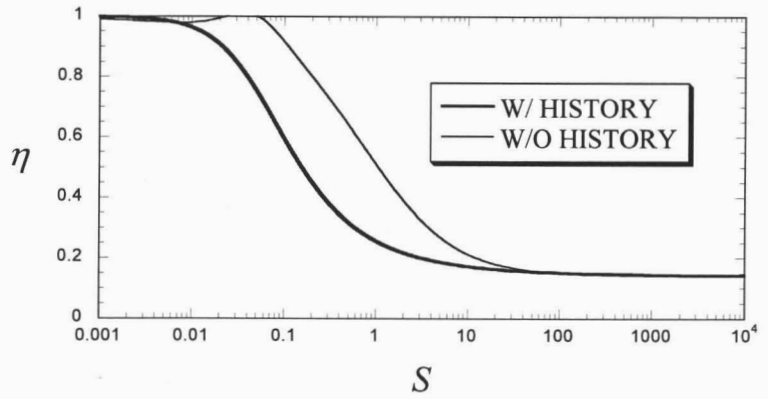

Figure 14. Amplitude ratio for α = 0.1.

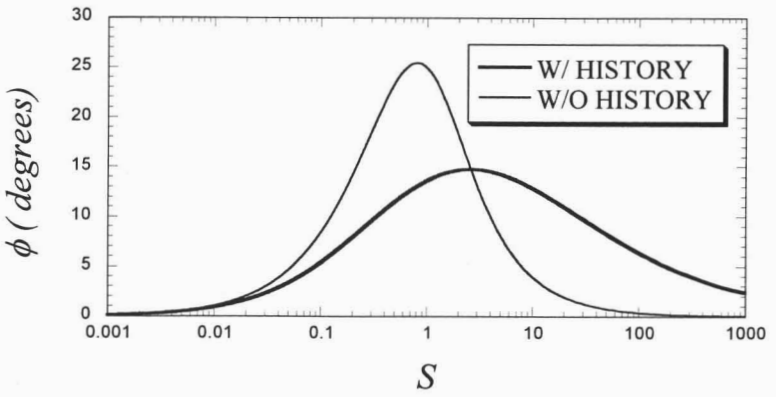

Figure 15. Phase difference for α = 1000.

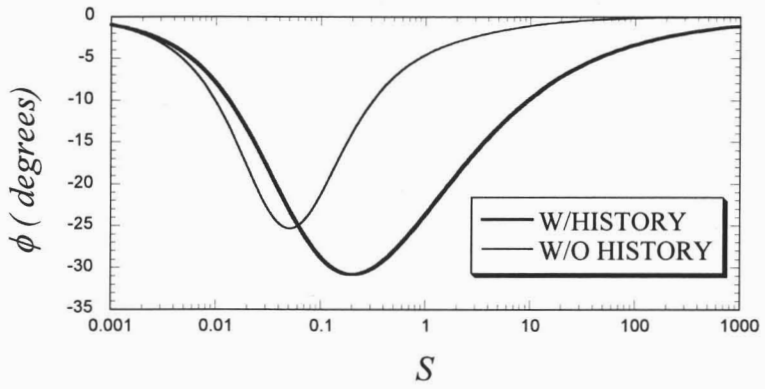

Figure 16. Phase difference for α = 0.1.

EXPERIMENTS

The experimental program involved three separate but related parts:

1. *Exploit existing spaceflight data that exists in the form of holograms by employing the virtual spaceflight chamber concept* - These studies are providing knowledge about particle movement in fluids and observation of quasi-steady g and g-jitter effects using existing holograms from Spacelab 3 and IML-1. The experiments are also providing information to aid the design of new ground and spaceflight experiments. These studies lead to a set of recommendations of how to improve the data quality in upcoming spaceflights.
2. *Conduct new Ground Experiments* - These studies will expand on the experiments from IML-1 and SL3 and will provide knowledge that will help design a spaceflight experiment. They are providing limited testing of the new solutions to the equations of motion.
3. *Flight Experiment* - Design an experiment that uses all of the knowledge gained in the program to attain the stated objectives.

PARTICLE FIELD HOLOGRAPHY AND VELOCIMETRY

All of the experiments involved the use of the various techniques of holography and resulted in advanced measurement techniques. Holography is an ideal method for recording the three-dimensional position of a distribution of small particles in a volume. In some cases, the particles themselves are the focus of attention. In other cases, the particles are used as a tracer for monitoring fluid motion. Holographic particle image displacement velocimetry (HPIV) has been in use for over thirty years[34,35,36] and has continuously undergone refinement as improved lasers

---

[34] J.D. Trolinger, W.M. Farmer, and R.A. Beltz, "Multiple Exposure Holography of Time Varying, Three-Dimensional Fields", *Applied Optics* Vol. 7, No. 8, pp.1640-1641 (1968).

[35] R.J. Adrian, "Scattering Particle Characteristics and their Effect on Pulsed Laser Measurement of Fluid Flow: Speckle Velocimetry vs. Particle Image Velocimetry," *Applied Optics* Vol. 23, pp. 1690-1702 (1984).

and imaging processing became available. Data reduction methods to derive velocity include: particle image tracking, image cross-correlation[37] and auto correlation, and Young's fringe analysis. Many procedures have been devised to enhance image quality and data quality[38].

OBSERVATION OF G-JITTER, RESIDUAL G, AND MICROCONVECTION FROM PREVIOUS IML-1 SPACEFLIGHT.

The IML-1 experiment incorporated tracer particles in the fluid surrounding a growing TGS crystal for the purpose of observing micro convection and effects of residual acceleration on crystal growth. The experiment produced over a thousand holograms of particle fields in a liquid. Polystyrene particles with nominal diameters 200, 400, and 600 microns were placed in a TGS solution in the FES (Fluids Experiment System) cell, which was a cube, approximately 10 centimeters, with glass walls on four sides. Holograms were made with time separations of about 10 minutes for periods up to 40 hours. The data was extracted from these holograms in the HGS (Holographic Ground Station). Data to support the crystal growth experiment was extracted during the IML-1 program. Later during the SHIVA project, additional data reduction software and analysis techniques were developed and used to further exploit the holographic data. The position of all the particles in the FES cell and all holograms (about 200 particles) were catalogued and used to compute residual acceleration, convection, and g-jitter. The following discussion describes some of the methods, interpretations, and information that will also be useful in the planned spaceflight.

Figure 17 illustrates the movement of a particle pair in a fluid under the influence of microgravity. In a low Reynolds number situation, the two particles within 10 diameters of each other can have a strong influence on each other. For example, a large particle can pull a small one along with it. Likewise, a wall within 10 diameters can have a strong influence of the motion of the particle. We have been able to observe these effects within the IML-1 data set but the experimental conditions were not sufficiently controlled to accurately quantify them, since this was not the objective. Additional data will be needed to fully understand such effects. With the data collected, we were able to identify particles that were isolated from the influence of surrounding particles.

If a particle's motion is not influenced by the motion of neighboring particles, then the effects of different types of forces can be observed directly and separated by understanding how the radius separating the particles changes. When the fluid has a convective velocity, all particles will attain the velocity of the fluid superimposed on the drift velocity (caused by gravity) in a short time (less than a second) after the fluid velocity changes. The particle separation remains constant under such forces (**Figure 17a**). Under constant acceleration (e.g. residual gravity) particles that are heavier (lighter) than the fluid attain a drift velocity in the same (opposite)

---

[36] J.D. Trolinger, R.B. Lal, D. McIntosh and W.K. Witherow "Holographic Particle Image Velocimetry in the First International Microgravity Laboratory aboard the Space Shuttle Discovery", *Applied Optics*, Vol. 35, No. 4, pp. 681-689 (1 Feb. 1996).

[37] J.M. Coupland, and N.A. Halliwell, "Particle Image Velocimetry; three dimensional fluid velocity measurements using holographic recording and optical correlation" *Applied Optics* 31, pp. 1005-1007, (1992).

[38] D.H. Barnhart, R.J. Adrian, and G.C. Papen, "Phase Conjugate Holographic System for High Resolution Particle Image Velocimetry" *Applied Optics* 33, pp. 7159-7170, (1994).

direction of acceleration that is proportional to the square of the diameter and proportional to the particle-to-fluid density ratio minus one. The calculated terminal velocities range between .01 to .04 mm/hr at 10^{-6} g's. Consequently, the separation of a large and small neighboring particle changes under the gravitational force. The rate of change of separation is a direct measure of g (**Figure 17b**). Vortical flow will manifest in a rotation of the radius separating the two particles without a change in length (**Figure 17c**).

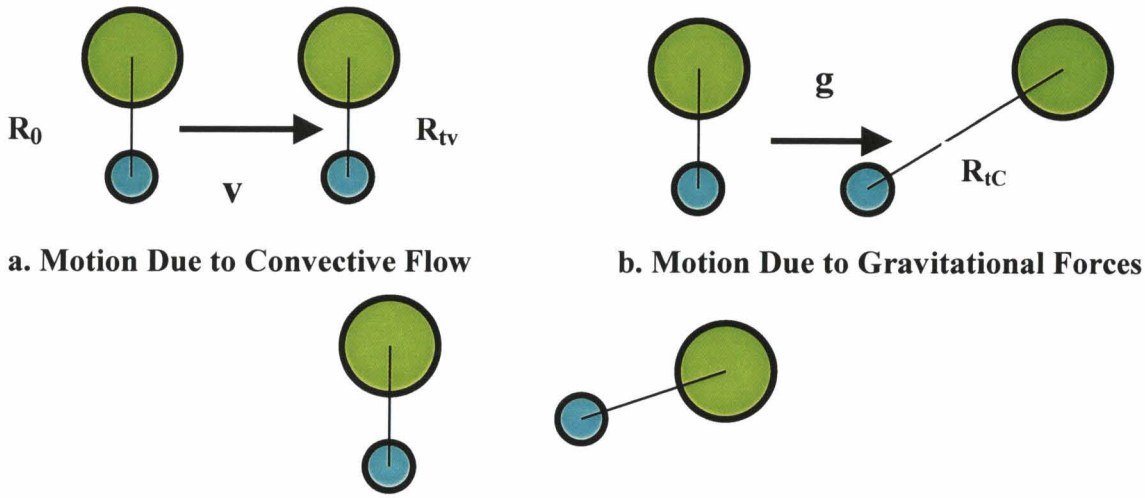

a. Motion Due to Convective Flow

b. Motion Due to Gravitational Forces

c. Motion Due to Vortical Flow

Figure 17. Motion of large and small particle pairs as influenced by gravity and convection.

- Under a force that varies sinusoidally in time, particles will move in a nearly sinusoidal fashion with an amplitude that is smaller (larger) than the fluid and a phase that lags (leads) the fluid for particles that are heavier (lighter) than the fluid. Lighter (Heavier) particles will track the flow more (less) closely than is predicted by most commonly used approximations.
- Under g-jitter, all particles should follow a similar movement with particles heavier than the fluid moving in opposite directions from those that are lighter than the fluid. The g-jitter accelerations range from a few micro-g's to milli-g's.
- A spacecraft maneuver will change the direction of g, consequently changing the gravitationally-induced velocity direction.

An accurate method for measuring g is to measure the separation between two particles of different mass. This method is self-compensating for many of the errors that are present when the movement of a single particle is use to compute g. For example, registration errors for the different frames containing images at different times is automatic with this procedure.

A random movement of particles in microgravity, under the influence of g-jitter, termed "inertial random walk", has been predicted, but not observed[39]. Most of the sources of g-jitter act within a closed system; that is, each force in one direction is followed by an opposing force. For example,

---

[39] L.L. Regel, A.A. Vedernikov, R.V. Ilinski, and M. Melikhov, "Analysis of Inertial Random Walk of Particles in Liquids under Microgravity Conditions", Proc. 6th European Sym. on Mat. Science under Microgravity Conditions, Bordeaux, France, Dec. 2-5, pp. 593-599 (1986).

if an astronaut pushes himself away from one side of the laboratory, he then is ultimately stopped by the opposing wall where his momentum returns to zero in the laboratory axis. When such a force moves a particle in one direction, a restoring force returns it to its original position. (If the initial action and restoring forces are vastly different in magnitude, a net particle movement is possible.) The effect of thrusters on the particle motion is slightly different because each thruster can change the momentum of the Space Station by forcing compressed gases to leave the closed system. So, the thruster action can cause particles to move somewhat randomly. Even so, the objective of using thrusters is to maintain the attitude of the Space Station constant with a tolerance, so these forces also approximately cancel out over a long time (except for maneuvers). We are designing part of the spaceflight experiment with the required sensitivity to observe inertial random walk.

We developed various methods using the IML-1 holograms for measuring and presenting microgravity effects on a particle field. Some of these methods will be applied to the planned spaceflight data and have been useful in planning the experiment.

Holograms of various types were recorded in IML-1. These included off-axis, in-line, diffuse backlight, direct backlight, and scattered light. Availability of this data has allowed us to compare the various methods and will help us make an optimum choice for the flight design.

Figure 18 is a reconstructed image of a plane of a particle field from an IML-1 hologram using diffuse backlighting. The background becomes a speckle pattern. Out-of-focus particles disappear into the speckle pattern within about a mm of traverse through the image. This makes automated image processing considerably simpler. The white dot appearing in the center of the image is an image of the light passing through the particle and it expands quickly out of the plane of the particle. Therefore, it is a clear indicator of best focus and can be used for automatic focusing.

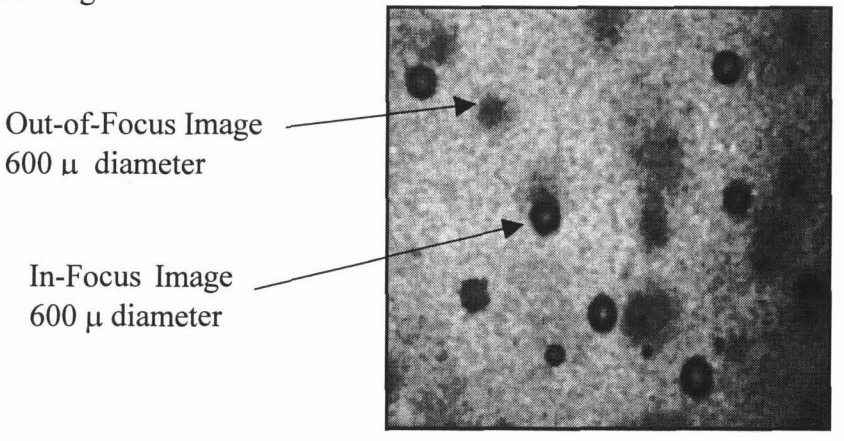

Figure 18. Reconstructed image with diffuse backlighting.

We developed an automated image analysis system that locates the position of best focus for each particle image and provides the precise *x,y,z* positions of all particles in the three-dimensional image. This is done for all holograms providing a high-resolution track of each particle as a function of time. We have developed various methods for presenting the data in one, two, and three-dimensional representations, depending upon the requirement. **Figure 19** and **Figure 20** provide examples of one-dimensional representations of the *x* and *y* positions as a function of time for an approximate two-hour period. The different curves represent the motion

of different particles. The movement of the various particles is more or less correlated as would be expected. These show the integrated effects of g-jitter with an approximate time of 10 minutes between position measurements.

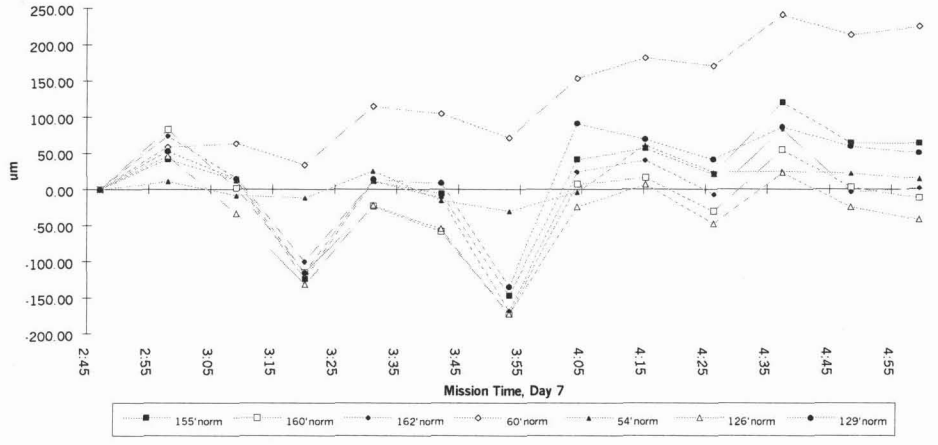

Figure 19. X displacement as a function of time.

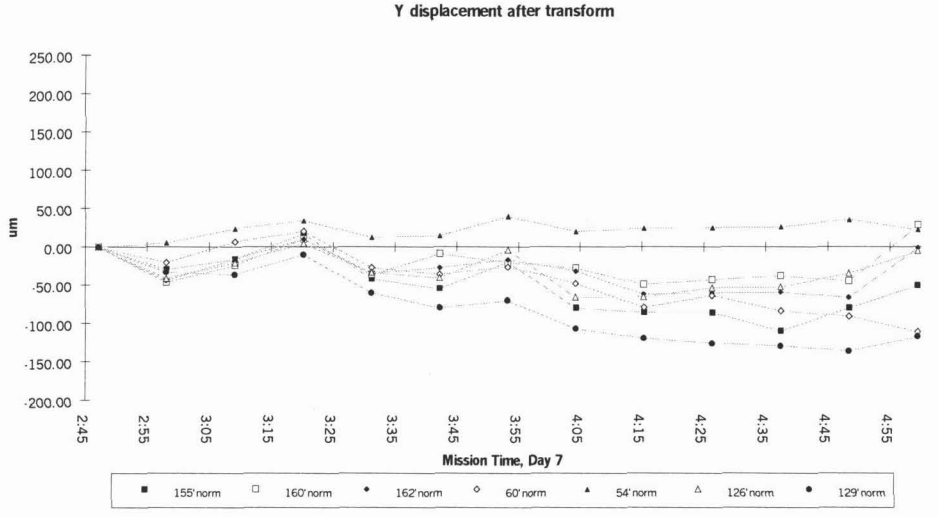

Figure 20. Y displacement as a function of time.

Several of the particles, which come from different places in the crystal growth chamber, exhibit coordinated motion, representing a direct observation of g-jitter, apparently the first ever to be made. A direct measurement of residual g is indicated by the observation that the particle position does not average to zero.

Using the equations of motion to determine residual g, data for a 14-hour time segment showing the effects of shuttle maneuvers is presented in **Figure 21.** The residual gravity in the direction of the sensitivity of the measurement is close to zero before and after the maneuver. Between the maneuvers, residual gravity averages to approximately 2 micro-g's. The maneuvers, marked on the graph, are clearly observable and correspond to data provided by NASA's Space Acceleration

Measurement System (SAMS). An extra acceleration event, also shown, was also observable by SAMS.

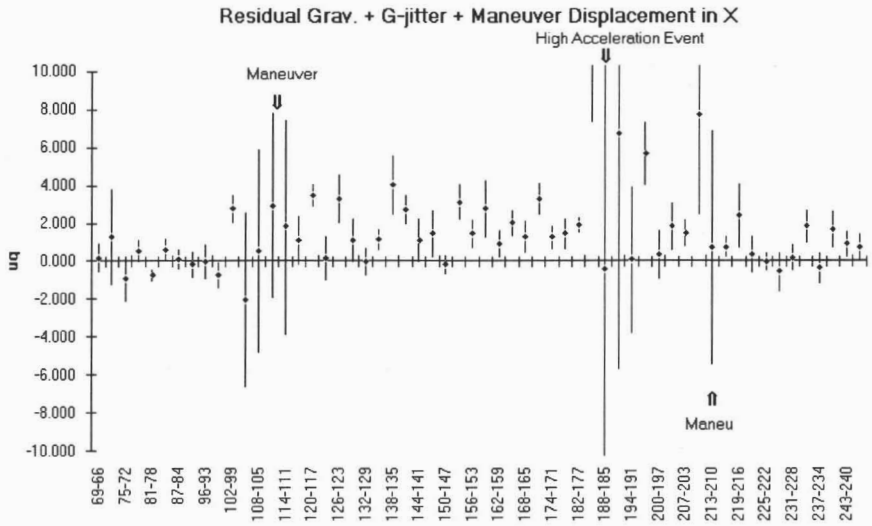

Figure 21. Residual gravity as a function of time, showing the effect of maneuvers. SAMS data was not available.

The data can be used to produce a convection map by sampling a few particle positions taken over a period that is short compared to the time in which convection is expected to change. Effects of shuttle maneuvers on convection could clearly be detected. **Figure 22** is a convection map drawn using this procedure taken from data after a several-hour settling time. The map shows a large-scale vorticle flow.

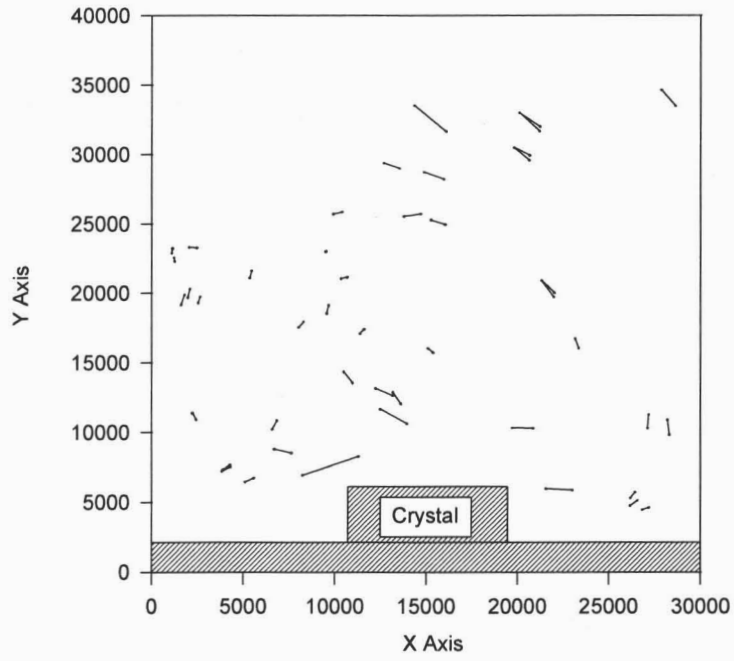

Figure 22. Microconvection before a maneuver.

Figure 23 shows the change that takes place in the pattern immediately after a maneuver. The flow field is much less defined, representing a type of micro-turbulence caused by the maneuver.

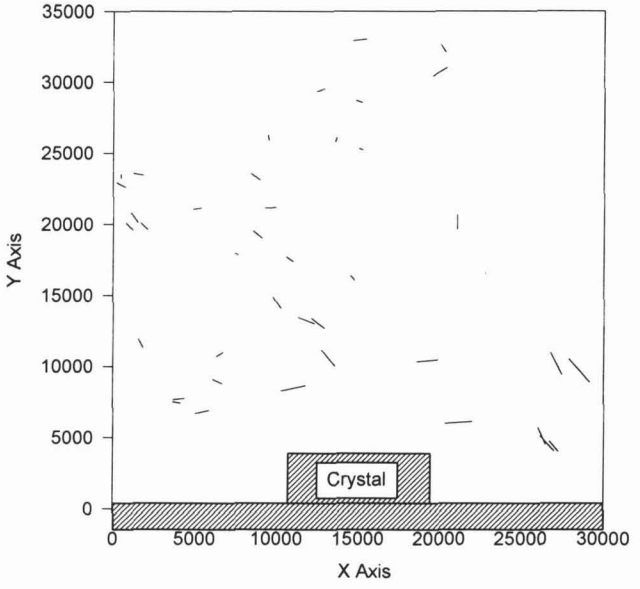

Figure 23. Microconvection immediately after a maneuver.

Figure 24 shows the results of relative motion tracking for an extended time. The direction is the same for all particle pairs. The anomalous behavior of the one particle shown in the third quadrant was interpreted as a particle interaction.

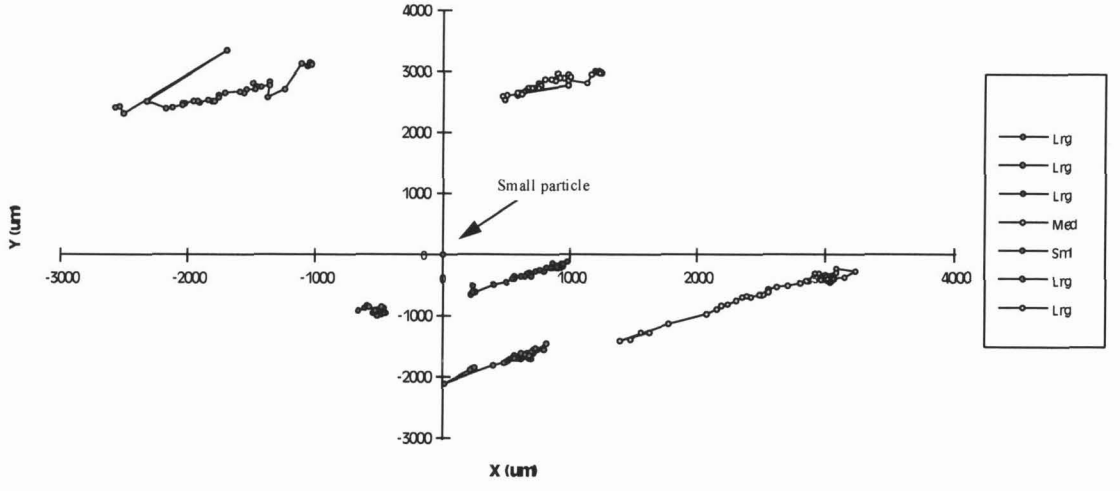

Figure 24. The relative motion of large and small particles.

RECOMMENDATIONS BASED ON ADDITIONAL STUDY OF IML-1 AND SL3 DATA

The incorporation of tracer particles in the IML-1 experiment achieved the goal of mapping micro convection and monitoring quasi-steady residual acceleration and provided useful data on particle and fluid interaction. Because this latter aspect of the project was a secondary objective,

the experiment design did not allow for certain types of measurement that can be made in an experiment that is especially designed for this purpose. Given the opportunity to design an experiment that can be focused on particle/fluid interaction and residual acceleration measurement, a number of recommendations can be made based on the experience gained from analysis of the IML-1 data. These can be summarized by the following:

1. Higher spatial resolution is needed to improve the accuracy and temporal resolution of the measurements of residual acceleration. An order of magnitude improvement in resolution can easily be attained with a specialized design. Because holograms were required to be located at a larger distance from the particles in IML-1 (in addition to other factors) spatial resolution was compromised. Holograms should be located as close as practical to the particle field.
2. A smaller chamber will allow full coverage of the chamber with small format film and a closer proximity of the holograms to the particle field.
3. IML-1 produced a variety of hologram types, including diffuse backlit, direct backlit, off-axis, in-line, and scattered light. For the proposed study, in-line holograms, which are the simplest, most robust holograms can provide the required data. This will allow a much simpler optical design, lower laser power, and a closer proximity of the hologram to the particle field.
4. Sets of multiple exposure holograms can provide velocity information efficiently with a saving of film.
5. It is extremely important to have distinct, accurate reference marks on the cell to allow calibration in the final holographic image.
6. The cell should be made with single, anti-reflection-coated windows that can be maintained clean.
7. Time identification marks on the film are important for correlation with Space Station events.
8. Fewer particles should be used to provide better data on particles without interaction.
9. Some cases of large particles, much heavier and much lighter than the fluid, should be studied to enhance sensitivity of the measurement.
10. Uniform density needs to be assured for some cases.

GROUND EXPERIMENTS

Although theoretical work has been performed on convection in microgravity with g-jitter, few experimental data are available to confirm or disprove predictions being made from such theories. This research has provided some of the first data in this area, as well as a tool for studying such effects in fluids; however, the available data from previous spaceflights do not provide the accuracy needed or the type of data needed to fully test the equations and produce accurate, time-resolved acceleration measurements. The proposed flight experiment will provide data that are more accurate and which are also carefully selected to achieve the goals of the project.

Measurement of the quasi-steady acceleration environment has been at least a part of the objective of many other studies such as OARE (Orbital Acceleration Research Experiment, MAMS (Microgravity Acceleration Measurement System), SAMS II (Space Acceleration Measurement System), and PAS (Passive Accelerometer System). The accuracy of all of these

instruments is highly questionable in the quasi-steady region because of the methods required to calibrate the devices. The procedures for calibrating and determining zero offsets are extremely tedious and subject to error. Other methods are needed for comparison.

PAS was developed and deployed in USML-1 and also on the MIR Space Station to measure quasi-steady acceleration.[40], using a method that is similar to that planned for SHIVA. A steel sphere was placed in a fluid-filled cell and the position of the sphere was monitored over a period of time for the purpose of making a direct measurement of residual acceleration. The tube was oriented manually with its long dimension in the expected direction of residual gravity. Measurements ranged between 0.05-2 micro-g's on MIR. Many good measurements were made as well as many that contain anomalies. Anomalies in the measurement have been given several possible sources, including magnetic interference and inertial drag variations. The PAS is a simple instrument that provided interesting measurements; however, much more accurate positioning and elimination of questionable wall effects are needed to make the measurement more meaningful. Measurements in the Space Lab showed considerably higher g-levels for some measurements, averaging above 4 micro-g's, while in other cases, measurements fell below 1 micro-g. These measurements clearly show the need for better time resolution as well as positional resolution to make this type of measurement most useful.

TESTING THE ANALYTICAL SOLUTION

The analytical solution to the particle/fluid equation of motion, developed during this research, was used to design both ground and flight experiments that will experimentally test cases that are significantly different from previously approximations and numerical solutions. Our solution shows that the history term cannot be neglected for many interesting cases (especially low Reynolds number cases). The terms become less important as the particle density approaches the fluid density where the particles rise or fall slowly enough to allow the experiment to be done on earth. A narrow range of conditions was identified where the usually negligible terms (that we will test in microgravity) are important even on the ground and can be tested in ground-based experiments. These are being used to gain experience and test the overall experimental concept before going to space. The primary objective of the ground experiment is to prove that we can locate the edge of a particle in a vibrating test cell with a precision sufficient to measure the effect of the history term on the particle amplitude. The required precision is about 10 microns.

The equations assume that we always maintain the condition of Reynolds number at less than 1. Very light or heavy particles rise or fall too fast in a fluid to maintain a low Reynolds number, and a factor of 2 in a density ratio between the fluid and particle is about the limit if the Reynolds number condition is to be maintained on the ground. To meet this condition requires that the amplitude of the sinusoidal motion should be about the particle diameter or less.

In ongoing experiments at MSFC and at MetroLaser, we tested various methods for launching particles, adding the vibration to the test cell and recording the particle in the fluid at the appropriate time. Experiments in both laboratories have been successful in showing that the required measurement precision is easily attainable using holographic recording.

---

[40] J.I. Alexander, Passive accelerometer system measurments on MIR, Final Report for PAS NASA 3, NAG8 1223 (1998?), J.I.A. and M.J.B. Rogers, NASA Conf. Pub. 3272, vol 2, pp 569-81, Joint L+1 Science Review of USML-1 and USMP-1 etc.

Based on the conclusions drawn from theoretical predictions and the fact that our particular interest is in the history term, we will run our experiments around the region where the scaling function $S = 1$ with $\alpha = 2$, and the optimum region for observing the history term effects peaks at about 60 Hz for this case. Although the optimum vibration frequency is about 60 Hz, it could lie between 10 and 100 Hz.

A specific case currently under test at MetroLaser is a 2 mm-diameter particle in a Krytox liquid filled cell that is shaken at frequencies up to 100 Hz with an amplitude of up to 0.3 mm. We have produced holograms that can be used to determine the amplitude of the particle motion with an accuracy of a few microns. Preliminary indications are that the results are predicted by our theory and the concept for the space flight experiment is valid.

The case of $\alpha\omega = 2$ ($S = 1$) (e.g., particle half the fluid density vibrating at 60 Hz.) provides nearly a 100% difference in the amplitudes with and without the history term. The effect would be more pronounced with yet a lighter (or heavier) particle, but this cannot be done easily in gravity. A vibrational amplitude of 100 microns should result in a 15 micron difference with and without the history term. We have shown in our ground experiments that we are at least a factor of 2 better than the resolution required to quantify the effect.

For the case we have chosen, the solution predicts that the particle will actually follow the fluid better than what is predicted by the approximations usually made. We have also arrived at the following conclusions from the analysis.

Two methods have been tested in this project.

1. In the same hologram, record two positions of the particle and a reference point on the cell, preferably when the cell position is at its extremes. This will allow us to make an accurate measurement of the fluid to particle amplitude. The fluid, being confined by the cell, will move by the same amount as the cell. The exposures must be short enough so that the particle does not move more than a few microns during the exposure. This will be most easily achieved at the maximum amplitude where the velocity of the particle and cell are at zero. It should be noted that the phase difference between the fluid and the particle is small enough to be neglected in making the amplitude measurements. This can be seen in **Figure 5** and **Figure 6**.
2. Produce a time-exposed hologram of the particle with an exposure that is long compared to the period of vibration. The edges of the elongated images should appear sharp since the particle is stationary at its maximum amplitude.

Only the first method is applicable on the ground since the particle will move too much, due to buoyancy, to maintain a sharp edge.

Figure 25 illustrates the experiment. The particle is released at the bottom of a fluid filled cell. The fluid is constrained to move with the cell. The cell is vibrated in a sinusoidal motion with an amplitude of 200 microns. Therefore, we can measure precisely where the fluid is at all times. As the particle rises, it attempts to follow the sinusoidal movement of the fluid; however, it follows a quasi-sinusoidal path with negative phase difference and larger amplitude (see particle and fluid motion in the figure).

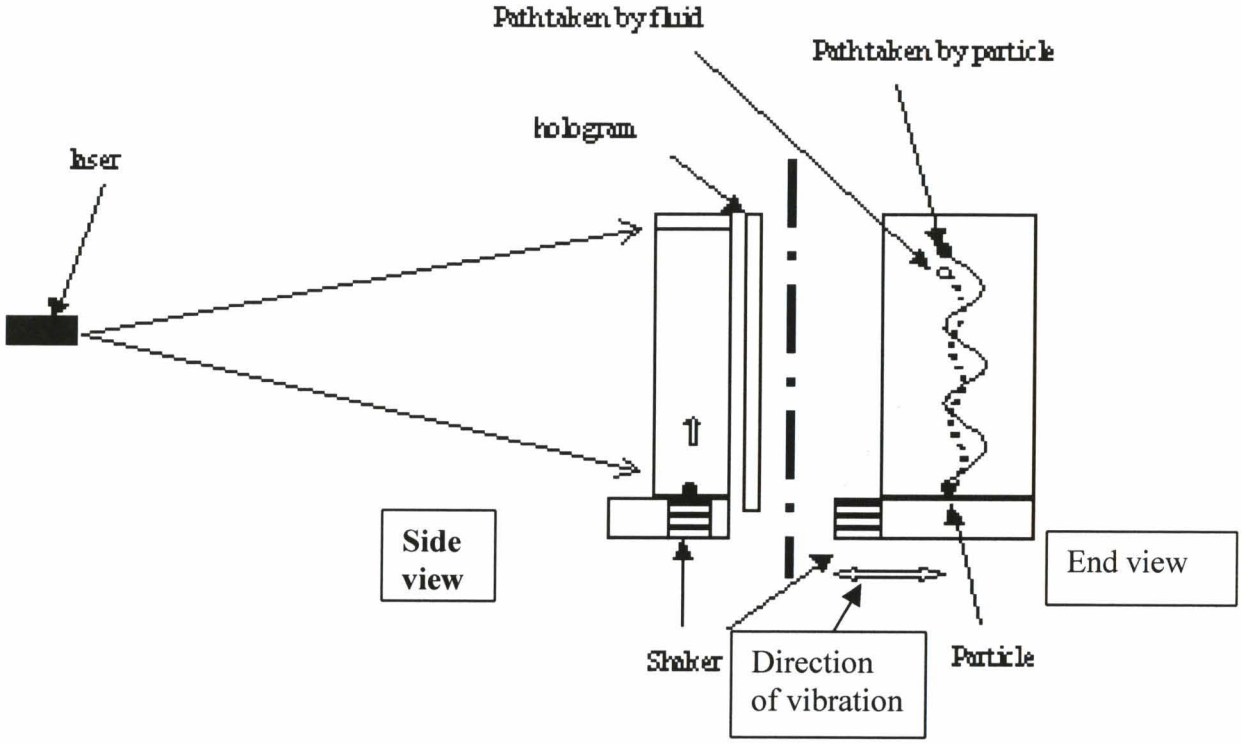

Figure 25. Ground experiment apparatus.

Figure 26 shows the actual experiment and the cell installed. The cell is mounted on a traverse to which a vibrator is attached shown in detail in **Figure 27.**

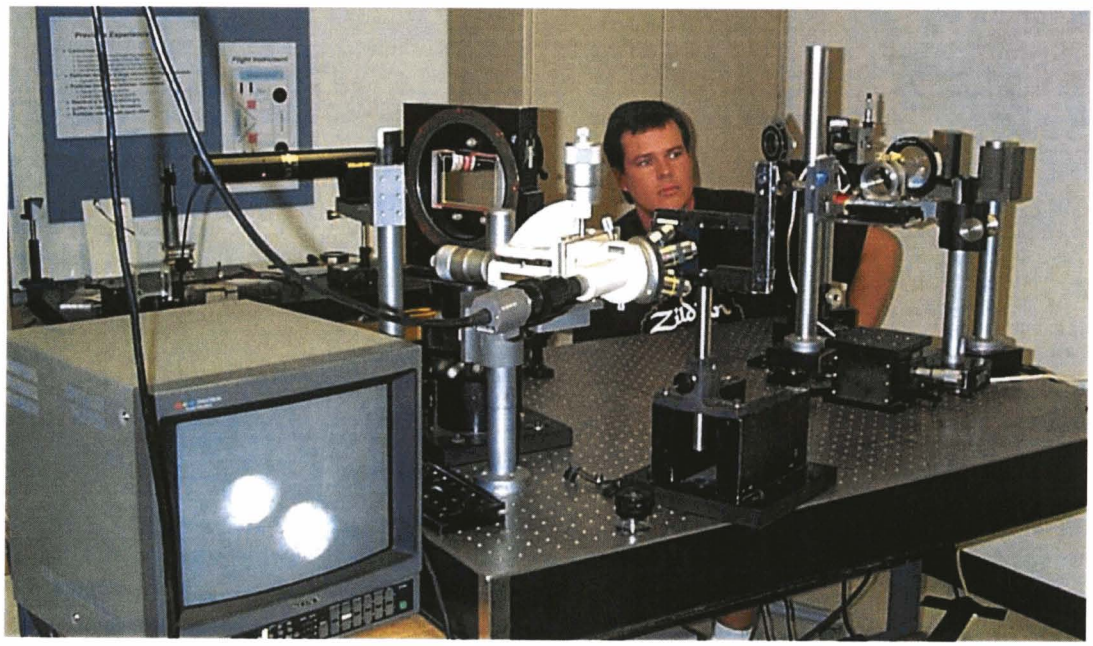

Figure 26. Ground experiment showing reconstructed images of a vibrating 2 mm diameter particle.

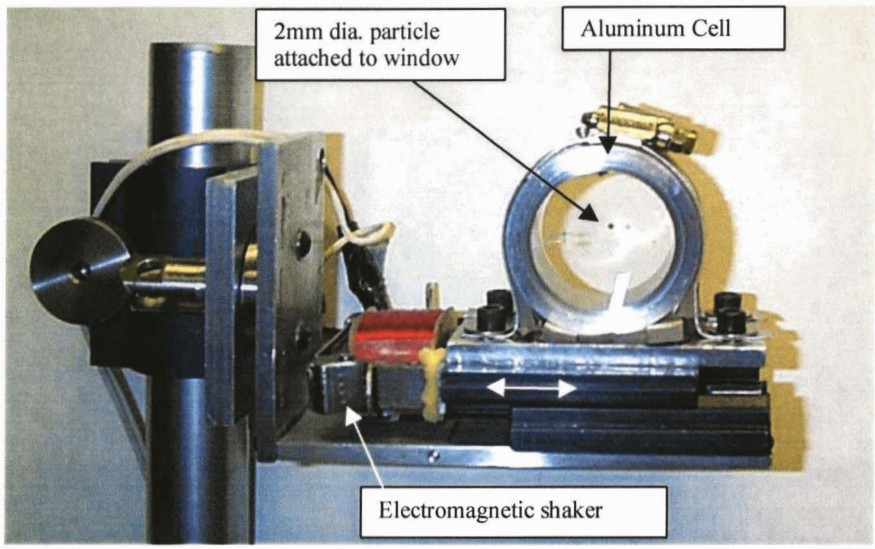

Figure 27. Cell and the shaker.

Figure 28 shows how the image of the sphere will appear when reconstructed from a hologram that is produced with an exposure that is large compared to the cycle of vibration. The different figures are for different amplitudes, *a*, relative to the diameter of the sphere. This analysis shows that the edge of the image, though lower in contrast, will provide a sharp marker of particle position at the maximum amplitude.

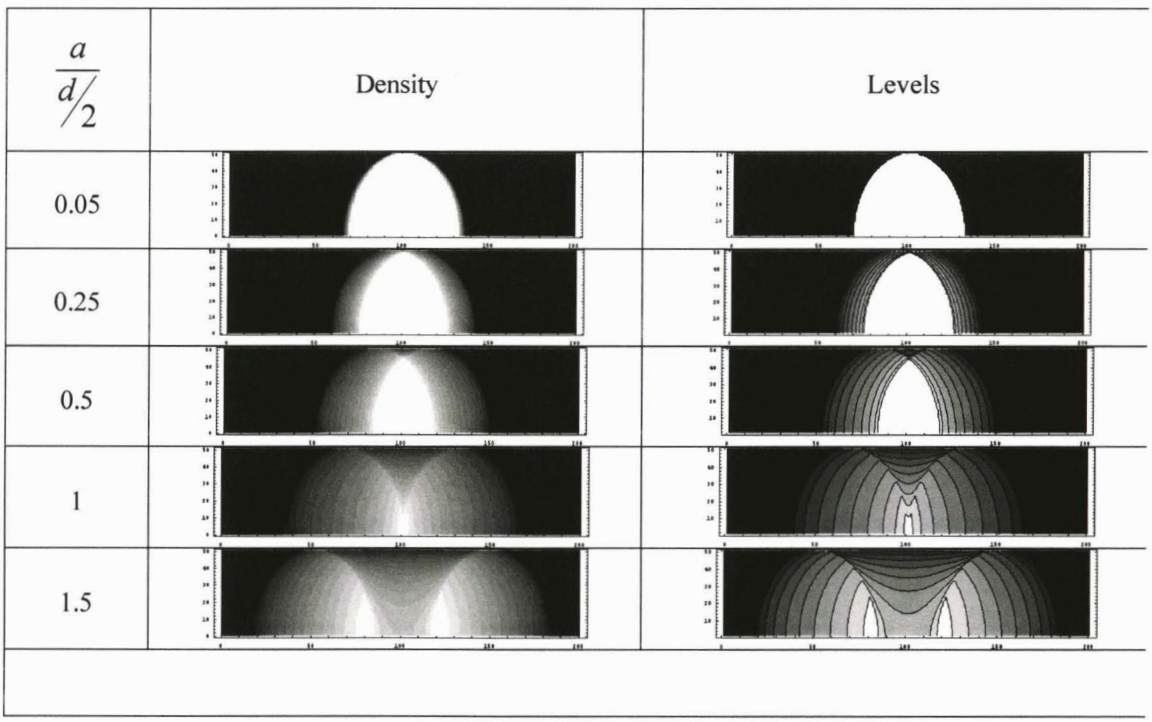

Figure 28. Theoretical appearance of a reconstructed image of a sphere where the exposure-time is long compared to a vibrational cycle. Figures are for different vibration amplitudes relative to the sphere diameter *d*.

We have produced holograms of a particle rising in a fluid-filled cell while the cell undergoes sinusoidal motion using both of the procedures described above.

The experimental parameters chosen for the ground experiment are the following:

- Particle Diameter: 2mm.
- Dupont Krytox®: 2gm/cc.
- Duke Scientific polymer particles: particle density one half the liquid density.
- Frequency of movement: 60 Hz.
- Amplitude of movement: $\pm$ 200 microns.
- Terminal velocity is about 2.5 cm/sec.

EXPERIMENTAL RESULTS

The simple method of making an exposure that is long enough to include one complete cycle was used to measure amplitude although the rising particle moves too much during the exposure to achieve the required resolution on earth. **Figure 29** shows a reconstructed image from a hologram of a particle in the cell and one fastened to the window vibrating at 60 Hz. The exposure lasted 1/50 of a second so that slightly more than one cycle was recorded. The edge of the particle on the window could be located to an accuracy of better than 10 microns while the rising particle edge was blurred severely.

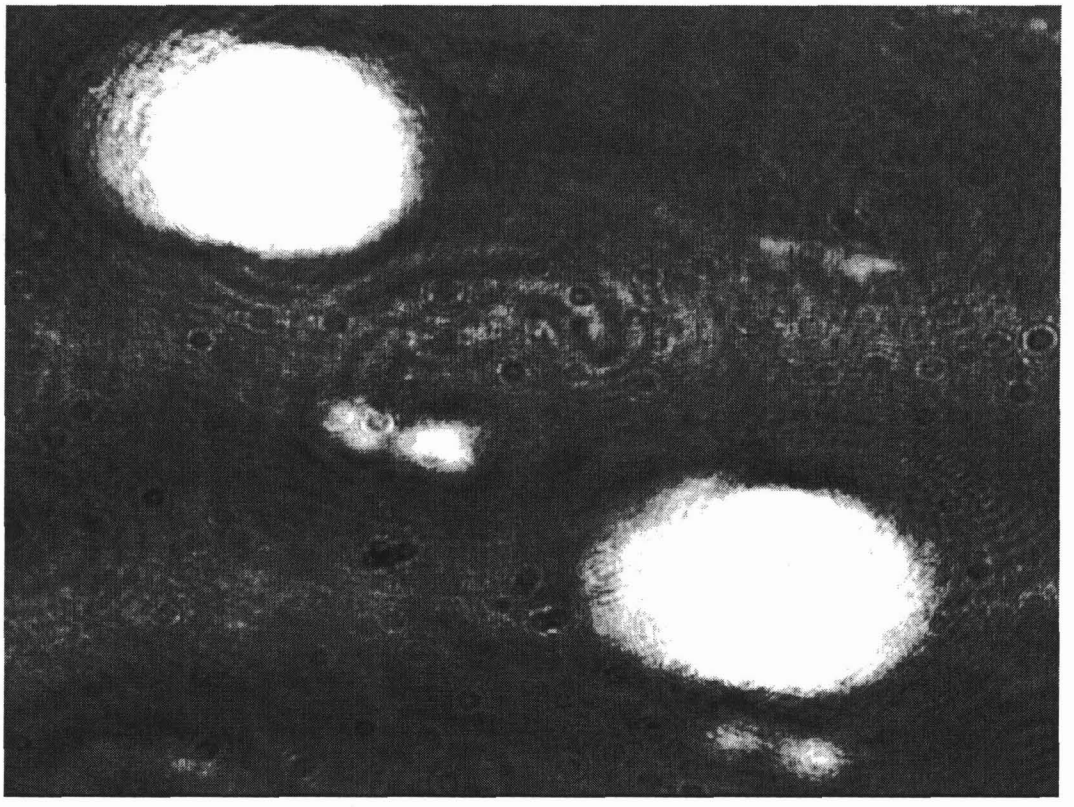

Figure 29. Reconstructed image from a time-exposed hologram of a vibrating particle. The image is focused on the particle attached to the window on the bottom right. Particles are 200 microns in diameter. Amplitude of vibration is about 500 microns. Smaller particles are air bubbles.

A few air bubbles are small enough that they move slowly enough to be in the picture. This may be a source of useful data in the final system.

Figure 30 shows the edge of a 2 mm-diameter particle reconstructed from a doubly exposed hologram where the particle is captured at its amplitude extremes. The amplitude of vibration is 100 microns. Clearly the center of the line representing the edge of the particle can be located to better than 5 microns, which is the desired resolution.

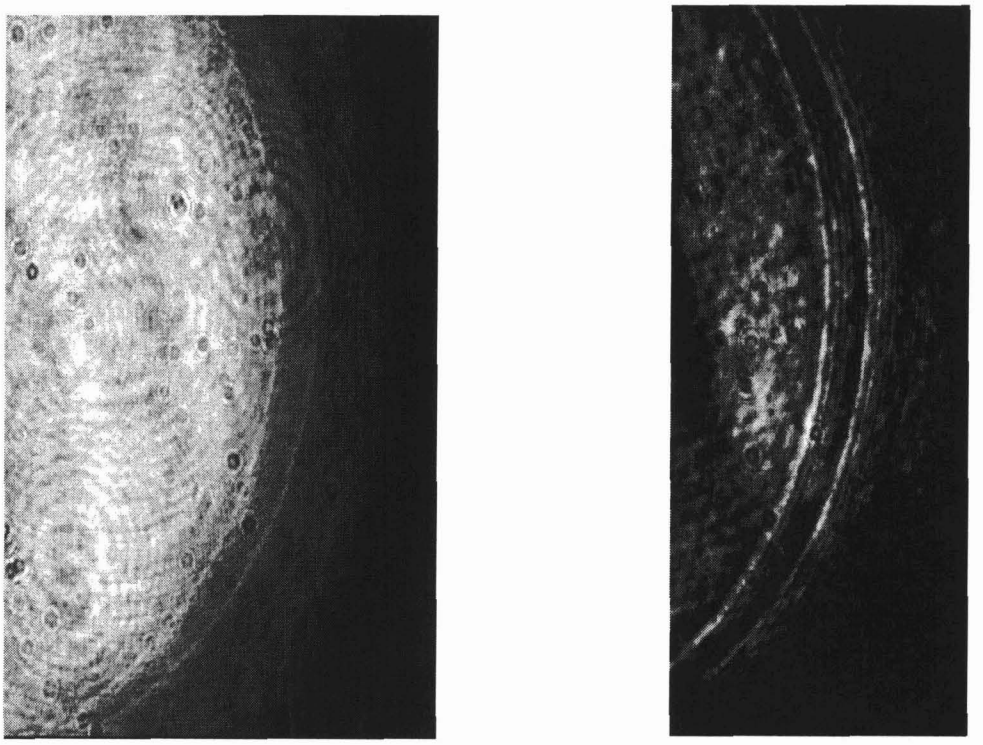

Figure 30. Reconstructed Image of the Edge of a particle from a doubly-exposed hologram. The particle moved 100 microns between exposures. The image in the right figure has been optically high pass filtered to enhance the edge image.

Figure 31 shows a comparison of the measured values of the amplitude ratio with the theoretical prediction. Agreement is within the measurement accuracy. Note that the history term is less important as the amplitude is increased as predicted by theory.

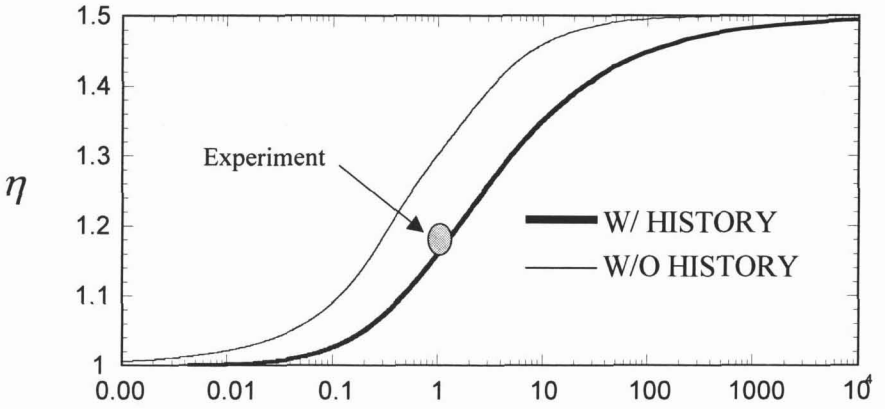

Figure 31. Experiment measurement of amplitude ratio.

FLIGHT EXPERIMENT DESIGN DATA

We have conducted preliminary experiments to select optimal components and configurations for an inline holocamera for the spaceflight particle tracking system. The approach was to set up a generic in-line holocamera using dimensions similar to what is anticipated in the spaceflight system and perform comparison experiments using the candidate components and configurations. We selected several slide-mounted particle sizes for hologram evaluation (e.g., 10-100 microns in diameter). Preliminary experiments suggest that diode lasers will be adequate for recording (see **Figure 32**).

The resolution measured in each of the cases was approximately 3 microns. Little difference could be detected in the resolution of HeNe recordings as compared with diode laser recordings. Therefore, we have chosen the diode laser as a light source because of its small size and power requirements.

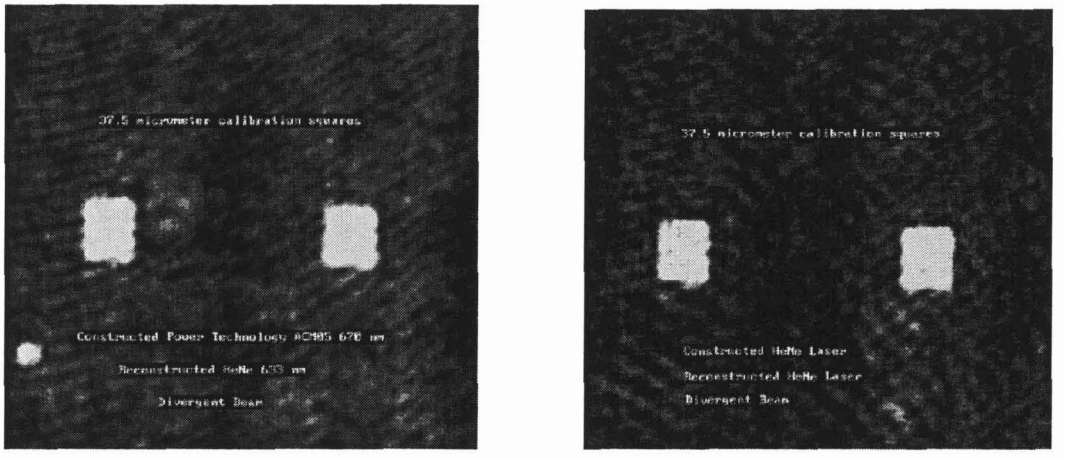

Figure 32. Comparison of images with laser diode holographically recorded and reconstructed image (left) and HeNe laser recorded and reconstructed image (right). Particle size is 37.5 microns. Diverging wave was used to record and reconstruct.

In our reconstruction system, the real image of the test cell is reconstructed into the field of an Olympus microscope to which a TV camera is attached. The microscope is programmed to move through the 3-D image, stopping to grab frames at predetermined positions. The images at preselected locations are digitized and stored for later analysis using a CCD (Charge coupled device) camera with a 512 x 480 pixel resolution. Afterwards, all images are analyzed to find for each particle where it reaches its best focus and the X-, Y- and Z-position is determined. With this database searching for specific particles (such as particles with no neighbors or particles near the wall), tracking becomes easy.

THE TETHERED PARTICLE METHOD

Another method for simulating the microgravity condition was developed. A hair was attached to the particle and the particle held in the center of the cell by attaching the other end of the hair to the bottom of the cell (or the top for heavy particles). This method appears useful for large particles. We collected data for 2 mm particles that is consistent with the free-floating particle. The procedure with this cell configuration is as follows:

1. Tethered particles float up or down depending on their densities. Krytox and steel particles are not being used.
2. The cell is inserted into the holocamera.
3. The vibrator shakes the cell at an amplitude that depends on the current.
4. The shaker is turned on.
5. A piezo-electric microphone is used to locate the position of the cell at all times.
6. The first holographic exposure is made when the cell reaches the maximum amplitude. A second hologram exposure is made when the cell reaches a maximum amplitude in the opposite direction. The exposure times are 1 msec.

The new cell was designed and constructed to test the interaction of particles with the walls and with each other. The cell was designed so that a wall could be moved closer and closer to the particle to evaluate wall effects. In addition, the design allows multiple particles to be tethered and observed. Either of these functions is difficult or impossible with the cells that have been used up until now since they have cylindrical walls and a small fill hole in the side. **Figure 33** shows the cell, which is a cube that is 4 cm on each side. The aluminum wall with a green sphere tethered a few diameters away can be observed. Another green sphere is shown tethered closer to the center of the cell.

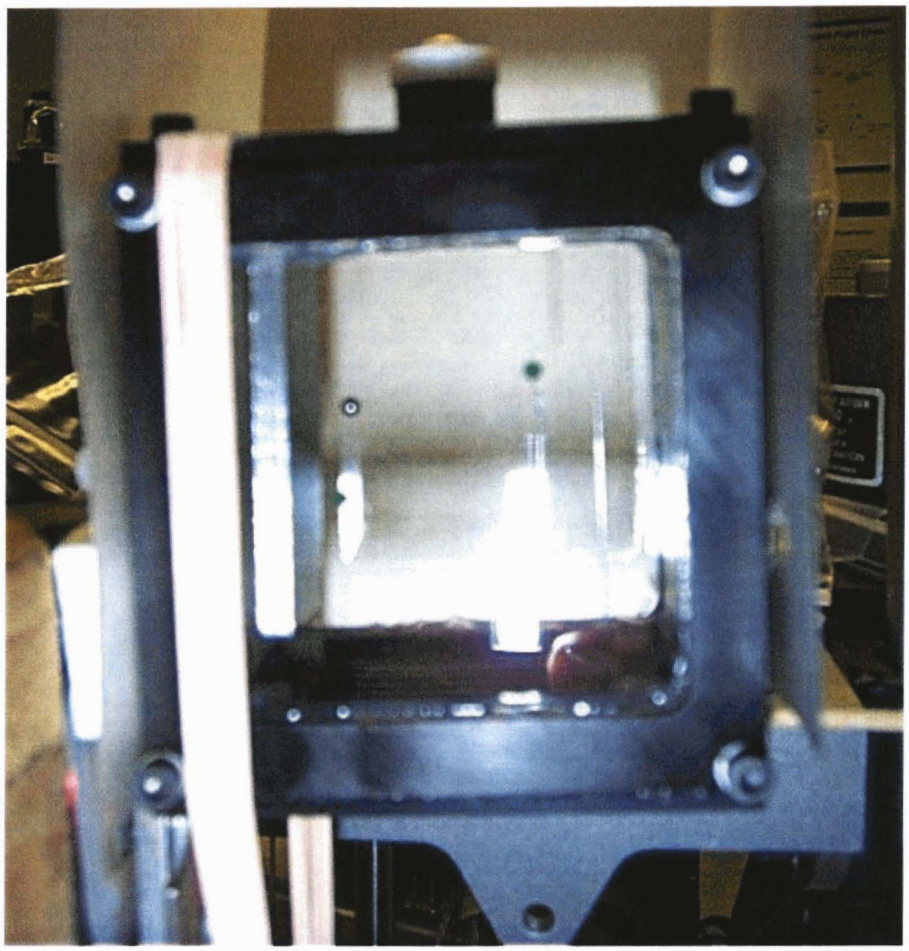

Figure 33. New cell design showing tethered spheres in Krytox.

Figure 33 shows an overall view of the cell and some peripheral components. The cell is held between two suspended vertical plastic sheets. The vibrator, which is hard-mounted to the table, is attached to the side of the cell. In previous experiments, we had some difficulty with the cell moving in an elliptical path instead of a linear one. This problem is mitigated by the rubber strap as it applies a force normal to the motion direction (see **Figure 34**). The amplitude of vibration is adjusted by adjusting the current to a variac that powers the vibrator and also by adjusting the tension in the rubber strap. With this setup, we can control the vibration amplitude continuously and maintain a linear movement of the cell. Amplitudes range between 10 to 100 microns.

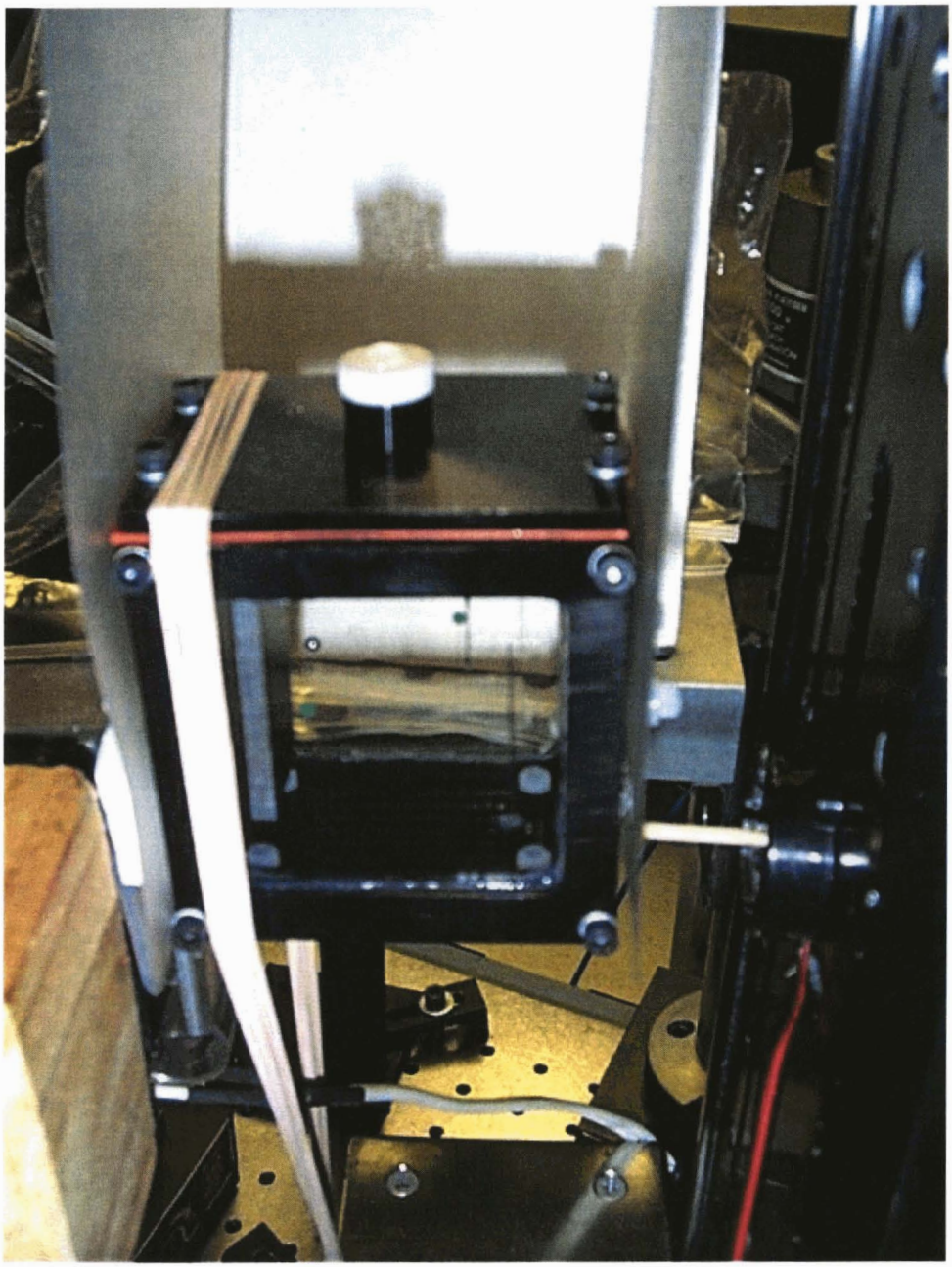

Figure 34. Overall view of cell showing rubber strap, vibrator, and position sensor.

In **Figure 34**, the vibrator is on the left of the cell and a piezo-electric microphone is shown attached to the cell on the right. The microphone allows us to monitor the exact position of the cell, providing a signal that is used to fire the shutter that records a hologram at the peak of vibration.

We improved accuracy of the measurement by placing scaling markers at various places in the field. In this current configuration, we can locate the edge of the sphere to within ± 3 microns. This is easily within the required range to observe the desired effects predicted by the Coimbra-Rangel solutions.

Figure 35 shows a plot of the amplitude of particle motion to fluid motion at various amplitudes. The slope of this line provides the predicted parameter, η. By taking several points on the curve to produce this value, the accuracy can be improved considerably to even better than what would be provided with the three micron position accuracy.

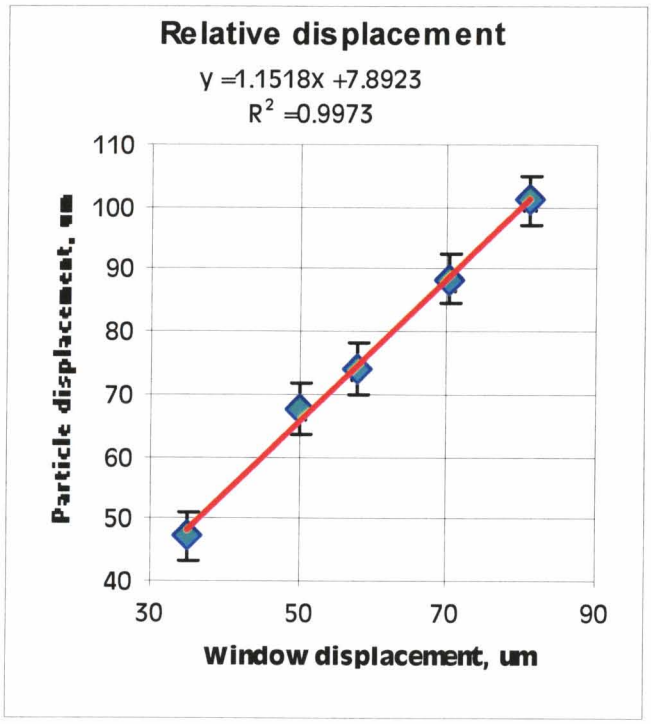

Figure 35. Ratio of particle to fluid displacement at 60 Hz vibration. The important number is the slope, or 1.1518. This number falls within 1% of the value predicted by the Coimbra-Rangel solution. The parameter S=1, and alpha=2.

The cell design has been under a constant evolution to improve experiment control and accuracy. The above procedure worked marginally and provided some of the first data; however, the apparatus was not flexible and also not precisely controllable. Controlling the amplitude and ensuring that the motion is rectilinear presented a challenge that required two more cell generations. This design evolved into the apparatus shown in **Figure 36 e)**. Bearing 1 (B1) is situated on the motor axes and the bearing axes is shifted from the motor axes on the value *a*. Rotating of the B1 with angular velocity Ω results in a displacement of the bearing's race in the same value and frequency Ω.

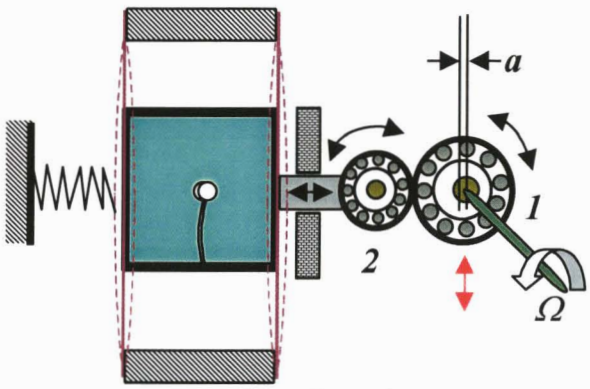

a) Cell and shaker configuration.

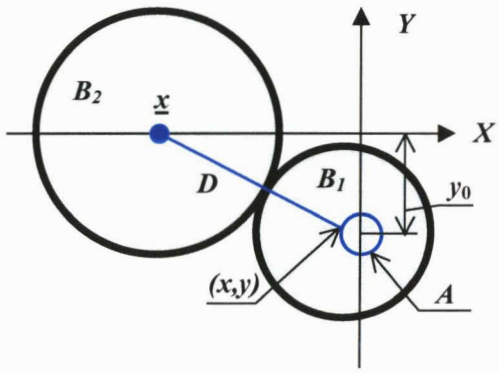

b) Coordinate system for solving of the B2 oscillation amplitude.

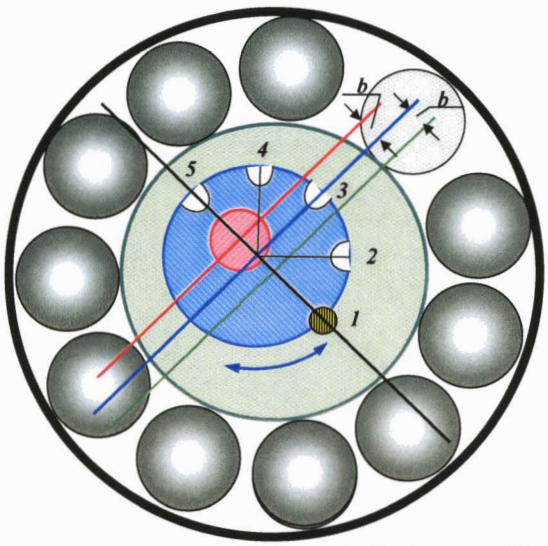

c) Design of the bearing 1 spindle. Key position 1-5 coincides the following amplitude of oscillation: 1 – a = 2×b; 2 – 1.85×b; 3 – 1.4×b; 4 – 0.77×b; 5 – 0×b.

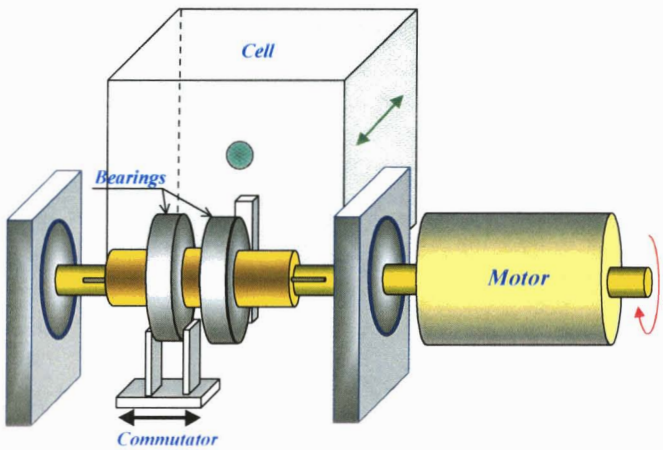

d) Gear shift design to change oscillation amplitude.

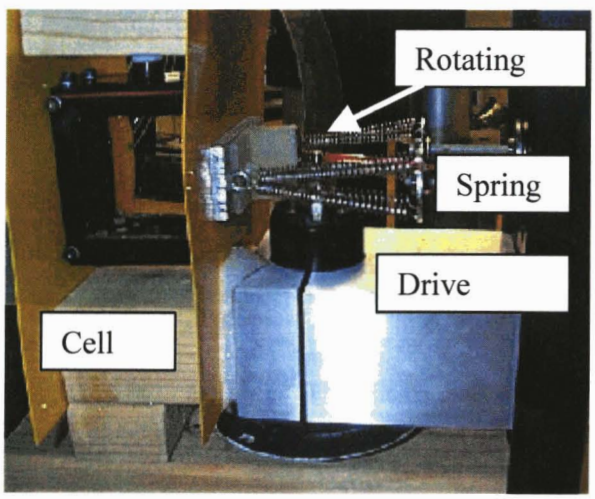

e) Experimental apparatus showing fluid-filled cell attached to a motor driven cam.

Figure 36. Cell schematic showing off-center cam concept, cam geometry and shifting mechanism.

Because the B1 rotation produces the motion of its race in two directions, a horizontal direction (relative picture), which is interesting for us; and a vertical direction, which we don't need, we will use the second, bearing 2 (B2), that is connected with the shaking object and eliminates vertical motion.

These two bearings reduce the friction effect and save energy. The shifting of B1 in a vertical direction (see the red arrow) allows for controlling the amplitude of shaking.
We can compute the requisite power for this system. If the mass of the shaking part is 500 g, a maximal frequency f = 80 Hz and a maximal amplitude 150 μm than maximal force F for shaking is:

$$F_{\max} = m \times \frac{dv}{dt} = m \times a \times \omega^2 \quad , \tag{24}$$

here v is maximal velocity of motion, m is mass of object, a is amplitude of oscillation, and $\omega = 2\pi \times f$. From **Eq. (24)** we have $F_{\max} \approx 19$ newtons = 2 kg. Power of the needed source of motion is

$$P_{\max} = F_{\max} \times v = F \times a \times \omega \quad . \tag{25}$$

So we have: $P_{\max} \approx 1.5$ W.

Therefore for oscillation of our object we have to spend power not less than 1.5 W because in this mechanical system there will be other losses of the energy. If in the worst case we have to spend 2 W power, that is not so bad. The motor for the rotation of our system will have a torque ($M = F \times a$) not less than 3×10^{-3} N*m. It is very small.

For estimating the cell motion, refer to **Figure 36 c)**. The distance between the centers of the bearings D = R_1+R_2 is consistent. Bearing 2 can move only in one dimension along X-axis. The axis of B1 moves along the circle A, which has radius a. We can write the equation describing describing the motion of B_2:

$$\underline{x} = x + \sqrt{D^2 - y_0^2 + (a^2 - x^2) \mp 2 \times y_0 \sqrt{a^2 - x^2}} \quad . \tag{26}$$

The rotation of B1 is described by the expression:

$$x = a \times \cos[\Omega t] \quad . \tag{27}$$

Because amplitude a is smaller than D, we can transform **Eq. (26)** and have

$$\underline{x} = \sqrt{D^2 - y_0^2} + \frac{a \times D}{\sqrt{D^2 - y_0^2}} \times \cos[\Omega t + \Phi]$$

$$\Phi = \arctan\left[\frac{y_0}{\sqrt{D^2 - y_0^2}}\right] \quad . \tag{28}$$

Equation (28) shows that B_2 oscillates on the same frequency Ω, but its amplitude depends on the displacement of B_1 from the axes X. When $y_0 = 0$, the amplitude of oscillating both bearings

is equal. For magnifying the amplitude of oscillation up to two times we need to use shifting $y_0 = 0.87\ D$.

We can use two-exocentric axes construction. The main bearing's spindle (green) contains a second spindle (blue), whose axis is shifted its axes from the axes of the main spindle by $a/2$. The motor spindle axes (red) is also shifted from the second spindle axes by $a/2$. In this design, the relative rotation of the second and main spindles results in changing the displacement between the motor and bearing axes. For fixation of the relative positions of the two spindles, we can use a key (yellow).

Dependence of the oscillation amplitude on angle θ of the relative angular rotation of the two spindles is

$$a = b \times \sin\left[\frac{\theta}{2}\right]. \tag{29}$$

In the caption of **Figure 33 c),** the values of the oscillation amplitude for a few positions of the key are noted.

The amplitude of the vibration is set by the cam offset and the frequency is set by the driving motor speed. Vibration frequencies up to 100 Hz at amplitudes up to 300 microns are easily achievable and accurately controllable with this apparatus.

Figure 37 shows a tethered 2 mm diameter polystyrene particle tethered on a 100 micron diameter fiber. The x positions designate the different positions of the sphere edge relative to an interacting wall. In this figure, the holograms are recorded at two times, when the sphere is located at extremes of the vibration. With this configuration, we have been able to examine many different types of particles and particle interactions.

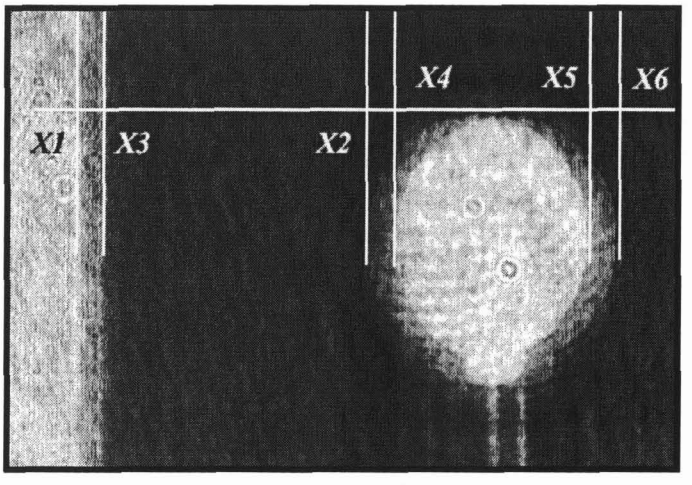

Figure 37. A tethered 2 mm diameter sphere undergoing vibration.

The experiment has repeated earlier experimental values for N = 1.15 and has also been used to examine wall interactions. Preliminary results suggest that the wall interaction is negligible for the 60 Hz case for particles coming within less than a mm from the wall.

FLIGHT EXPERIMENT DESIGN

The flight experiment design was started during this ground program and is currently continuing under the flight program. Below, the experiment as of December 2000 is presented.

EXPERIMENT PROCEDURES TO BE USED

The anticipated procedure is as follows:

- Place multiple particles, having the same density as the fluid, as tracers in an experiment cell to provide a baseline calibration of the cell dynamics. The movement of the particles will be observed over the operating conditions of the cell to detect any residual or induced convection present in the cell.
- Inject single particles near the center of a liquid-filled cell and track the precise location of the particle with holography while pre-programmed forces are applied to the cell.
- Apply forces on the particle by moving the cell sinusoidally and also with natural movement of the Space Station to which the cell is attached.
- Compare the movement of the particle with that of the fluid (cell).
- Track the movement of the particle in the fluid under the influence of the microgravity environment (i.e., g-jitter and residual g).
- Introduce multiple particles and a wide range of parameters.
- Observe wall effects as particles drift to the walls of the cell.
- Observe the movement of a real crystal in solution.
- Observe a depletion layer or similar gradient in the fluid around the crystal and its interaction with the moving particle.

MEASUREMENTS REQUIRED

The required measurements are:

- Particle position as a function of time.
- Particle vibration amplitude/cell amplitude ratio.
- Fluid temperature and temperature gradient.
- Density gradients in the fluid and depletion zone (or similar gradient) around the crystal.
- Acceleration environment.

We require measurement of the solution temperature with sufficient accuracy and resolution to allow for determining the uniformity of the environment and precise determination of the solution viscosity. Also, in the case where a temperature gradient is imposed, we require a measurement of the gradient.

We require a qualitative measurement of the fluid density gradients at least along the direction of the temperature gradient with wave shearing interferometry. This can be incorporated into the holographic system by inserting a shear plate in front of the hologram.

We require measurement of the acceleration in the vicinity of the experiment to compare with acceleration measurements that we compute. Of specific interest is the acceleration in the low frequency range below about 10 Hz. We also require measurements of the acceleration in the frequency range from 60 to 80 Hz so that we can know the relative influence of the environment in the range where we are applying acceleration to the cell.

ANTICIPATED PARTICLE MOVEMENT

In all of the cases we have selected for study, theory predicts that particles will reach their terminal velocity within a few milliseconds after injection or after a change in acceleration. Therefore, particles injected at the center of the cell will arrive at terminal velocity before moving very far. The table below gives the terminal velocity and the time required for a particle to travel from the center of the cell to a wall under the acceleration of one micro-g. Since we are anticipating about one micro-g of residual acceleration, we can conclude that without other forces the time required for particles to hit the wall in our experiment will range from a few hours to many days. This is consistent with IML-1 observations where particles were observed to remain in the field of view for many hours. It is also consistent with results described in the PAS report. Therefore, we expect most of our single particle cases to remain near the center of the cell for most of the experiment. The case, α=2, is represented by polystyrene in Krytox, while α=0.1 (α=1000) would be represented by a much heavier (lighter) particle. Therefore, our particle/wall and particle/particle interaction studies will be most likely to occur in the multiple particle experiments where many particles exist throughout the cell.

Terminal Velocity

The terminal velocity for the steady state case is the following:

$$V_t = \frac{(1-\alpha)a^2 gt}{\alpha\nu} \qquad \left(\frac{9.8\times10^{-6}}{\mu g_{earth}} \text{ m/sec}^2 \right),$$

where the factor in parenthesis allows g to be expressed in micro-g's.

Table 1. Terminal Velocity

Diameter	**Velocity** *(μ/sec)*		**Time to Reach Wall** *(sec)*	
(α=2)	**Krytox**	**Water**	**Krytox**	**Water**
2mm	.0272	1.078	$7.35\text{x}10^{5}$	$1.86\text{x}10^{4}$
200 μ	$2.72\text{x}10^{-4}$	$1.078\text{x}10^{-2}$	$7.35\text{x}10^{7}$	$1.86\text{x}10^{6}$
(α=1000)				
2mm	$1.36\text{x}10^{-2}$	$5.39\text{x}10^{-1}$	$1.47\text{x}10^{6}$	$3.13\text{x}10^{4}$
200μ	$1.36\text{x}10^{-4}$	$5.39\text{x}10^{-3}$	$1.47\text{x}10^{8}$	$3.13\text{x}10^{6}$
(α=0.1)				
2mm	$2.45\text{x}10^{-1}$	9.7	$8.16\text{x}10^{4}$	$2.06\text{x}10^{3}$
200μ	$2.45\text{x}10^{-3}$	$9.7\text{x}10^{-2}$	$8.16\text{x}10^{6}$	$2.06\text{x}10^{5}$

It appears that the sinusoidal forcing function is best choice for both the ground and spaceflight experiments. Particle amplitudes will range from zero, for heavy particles to three times the fluid amplitude for bubbles.

The variables have been integrated in terms of their role in the equation of motion in such a way to effectively reduce the number of experiments that will be required. We have reduced these to three parameters, α, Σ, and the Reynolds number that are defined in **Table 2**. Also the table

shows the desired range for testing for each parameter. A preliminary test matrix was produced, addressing the four parts of the test theme.

Table 2. Experiment Parameters

Parameter	Name	Desired Range of testing
$\alpha=\rho_\phi/\rho_\pi$	Fluid–to-particle density ratio	>20, 2, 1, 0.1
$\Sigma=\Omega\alpha^2/9\nu$	Scaling parameter	0.1, 1, 10
$Re=\alpha\omega/\nu$	Reynolds Number	0.1, 1, 10

Ω	=	Vibration frequency of the fluid
a	=	Particle radius
ν	=	Kinematic fluid viscosity = ρ_f/μ
μ	=	Static fluid viscosity
v_f	=	Fluid velocity
v_p	=	Particle velocity
w	=	v_f-v_p

At a minimum, our flight matrix should contain parameters that we tested on the ground plus cases that cannot be tested on the ground.

Table 3 summarizes an experimental set that would cover each of the parameters over a range of at least two decades. We will design our spaceflight experiment around this table.

Table 3. Range of Experiment Parameters to be tested.

	$\alpha=\rho_\phi/\rho_\pi$	$Re=\alpha\omega/\nu$	$S=\Omega\alpha^2/9\nu$
1	2	<<1	1
2	2	1	1
3	2	10	1
4	2	<<1	0.1
5	2	<<1	10
6	>20	<<1	1
7	0.1	<<1	1
8	1	<<1	1

There are 24 possible experiments here. There are ways to perform more than one experiment in any single cell. We have devised a set of experiments that cover most of these conditions. They are described in detail in the following paragraphs.

FLIGHT EXPERIMENTS (MODIFIED 21 MARCH, 2001)

Based upon extensive ground experiments and theoretical analyses, we have devised a comprehensive set of experiments with a sufficient variety of parameters to fully validate the new solutions. In addition, the experiment has been designed provide data describing common conditions that are currently unpredictable, even with the new solution so that, as the theoretical work evolves, new predictions can be tested with this data. The experiment will also provide accurate measurements characterizing the Space Station Acceleration environment and its effects on materials sciences experiments. The availability of such data will provide insights that can help theoreticians extend their current work.

The experiment begins with a baseline measurement, the main purpose of which is to establish the overall cell characteristics, behavior, and interaction with the Space Station. In addition the experiment will provide a wide range of information, including valuable science data. It contains a blend of particle sizes and densities, interaction events, and acceleration measurements. The experiments then move on to fundamental, single particle experiments, with highly controlled experimental parameters.

Experiments move on step-wise in complexity adding conditions that involve the more complex interaction of particles with other particles and the walls. A particle that is close to a wall requires a greater force to move it. Particles moving in a fluid at extremely low Reynolds numbers exert an influence that extends outward for many particle diameters. For example, a large particle moving through a fluid will drag a nearby smaller particle along at a much higher velocity than it would attain without the influence. Data is needed to help theoreticians in developing an understanding of such influences. These cases will be covered in three ways. As particles drift towards the walls, the wall interaction case will occur naturally. For the particle interaction case, a unique opportunity exists in space to study a lightweight particle and a heavy particle, thereby making the transition from interacting to non-interacting under the influence of residual acceleration, which provides a natural way to separate the two in time. This condition also provides the optimum for measurement of residual acceleration.

The equations under consideration here are valid when the Reynolds number is much less than one. This is the case for a wide range of experiments in space, since the particles move extremely slowly. The equations take on a new level of complexity for Reynolds numbers greater than one, and a solution does not currently exist. The experiments will include cases where Reynolds number conditions exceed the validity of the equations of motion that have been solved, providing a new database for investigators to advance the theory beyond the current state-of-the-art.

The assumptions in the current theory are not applicable to the case of bubbles. While it is of interest to extend the theory to cover bubbles, we have not included them as a part of the test matrix.

The following experiments have been selected for the test matrix:

Notes:

1. *Experiments are listed in order of priority, and priorities have been set according to which experiments attain the goals the quickest. A change in the order of experiments to save experiment time and complexity can be justified and will be acceptable in most cases.*
2. *The purpose of repetition in the experiments is for statistical improvement of data and for backup data.*
3. *It is anticipated that cells can be easily removed from the apparatus.*
4. *Cell replacement for each experiment is required only when particles are not visible near the cell center, when the fluid is changed, when preloaded cells are used, and when the temperature gradient is added.*
5. *Experiments may be combined and/or interlaced so that two or more conditions can be provided without a cell change. For example, vibration frequencies and amplitudes can be applied alternatively in the same experiment. While obtaining data at several frequencies may not be a high priority, it may save considerable experiment time to combine and perform such experiments in the same sequence.*
6. *The added vibrational forcing function is anticipated to be many times larger than the acceleration environment of the ISS. We believe that isolation of the experiment from ISS may not be necessary; however, since isolation is required for other parts of the experiment, it is prudent to include it also for the forced vibration experiments since we cannot be 100% sure that ISS effects are always negligible. Also, isolation from ISS will enable us to meet the "good neighbor policy" regarding effects of SHIVA on other experiments in ISS.*
7. *Downlink video data as soon as practical if not available in real time. Sets of data can be collected and downlinked as a group.*
8. *Short intervals of video can be used beneficially for experiment diagnostics and functional tests during changes and initiation of experiments and during particle injections.*
9. *Residual g measurements are best made with either the heavy or light weight particles. Measurements made with light particles provide the most sensitive theoretical checks. Both of these are desired to optimally complete all goals, but all goals can be attained with light particles.*

Experiment #0: (Baseline calibration)

Krytox filled cell containing twenty-five 2 mm diameter particles whose density equals the fluid density, twenty-five 2 mm diameter lightweight particles ($\alpha>20$), and twenty-five 200 micron diameter heavy particles ($\alpha<20$). Crew member should shake the cell to insure that particles can be seen visually throughout the cell.

Note: This experiment serves five purposes.

1. *Observe any unwanted currents caused by the forcing function.*
2. *Observe any unwanted currents caused by isolation/forcing function interaction.*
3. *Observe particle-wall interactions.*

4. *Observe particle-particle interactions.*
5. *Provide backup data for several other experiments.*

Experiment #0.A: (16 Holograms, 30 seconds of video) (Isolated from ISS)

1. Record a single exposure hologram on film and video. Begin recording 30 seconds of video.
2. Advance film and store (or downlink) video frame and 30 second video recording.
3. Begin vibration at 60 Hz. $\pm$200 microns.
4. Record double exposed hologram (on film and on a single video frame) with one millisecond exposure where the first pulse is synchronized with one vibration amplitude maximum and the second is synchronized with the opposite maximum and with both exposures occurring in less than one second.
5. Stop vibration.
6. Advance film and store (or downlink) video frame and video recording.
7. Repeat steps 1-6.
8. Wait five minutes.
9. Repeat steps 1-6.
10. Wait 30 minutes.
11. Repeat steps 1-9.

Experiment #0.B: (16 holograms, 30 seconds of video)

Repeat Experiment #0.A, except vibration frequency at 40 Hz.

Experiment #0.C: (16 holograms, 30 seconds of video)

Repeat Experiment #0.A, except vibration frequency of 80 Hz and $\pm$100 micron amplitude.

Experiment #0.D: (16 holograms, 30 seconds of video) (Not Isolated from ISS)

Repeat Experiment #0.A, except without isolation from ISS.

Experiment #1: (60 Holograms, five minutes of video) (Isolated from ISS)

Krytox filled cell.

1. Begin video recording; inject 2 mm, polystyrene particle near cell center.
2. Retract injection device by at least one cm away from particle.
3. Record single pulsed hologram on film and on video frame.
4. Advance film and store or down-link video frame and video recording.
5. Begin vibration at 60 Hz. $\pm$200 microns.
6. Record double exposed hologram on film and on video frame with one millisecond exposure where the first pulse is synchronized with one vibration amplitude maximum and the second is synchronized with the opposite maximum within 60 seconds of the first.
7. Stop vibration.
8. Advance film and store video frame and downlink.

9. Repeat steps 5-8 five times.

   9a. **(24 additional holograms)** Note: See Note 4 above-alternate frequencies and amplitudes can be inserted here depending upon the final experiment design. The following cases are to be incorporated somewhere in the experiments. Therefore, a likely optimum experiment design is to repeat steps 5-9 except changing frequency and amplitude of vibration to cover the following cases:

   - 60Hz., ±100micron amplitude
   - 60Hz., ±200micron amplitude (case covered by steps 5-7 above)
   - 40Hz., ±100micron amplitude
   - 40Hz., ±200micron amplitude
   - 80Hz., ±100micron amplitude

Note: (12 holograms for each case)

10. Record a double-exposed hologram with 5-minute separation between exposures.
11. Advance film and store video frame and downlink (if possible).
12. Record a single pulsed hologram.
13. Advance film and store video frame and downlink (if possible).
14. Repeat steps 10-13 every five minutes for two hours or until the particle strikes a wall.

Experiment #2: (84 Holograms, five minutes of video)

Same as Experiment #1 except with a lightweight, 2 mm-diameter particle.

Experiment #3: (84 Holograms, five minutes of video)

Same as Experiment #1 except with a heavy 2 mm-diameter particle (e.g. gold, platinum, tungsten).

Experiment #4: (84 Holograms, five minutes of video)

Same as Experiment #1 except with 200 micron diameter, lightweight or polystyrene (lightweight preferred) sphere.

Experiment #5: (31 Holograms, five minutes of video)

Same as Experiment #1 except for the following changes: Particle number: Inject two 2 mm diameter, lightweight particles within a 1 cm^3 volume near the cell center. The initial center-to-center separation between the two particles should lie in the range of 0.3-0.5 Cm. The line between the particle centers should be parallel to the vibration direction. The experiment should be terminated after step 9a.

Experiment #6: (31 Holograms, five minutes of video)

Same as Experiment #5 except the initial center-to-center separation between the two particles should lie in the range 0.5-1.0 Cm.

Experiment #7: (84 Holograms, five minutes of video)

Same as Experiment #1 with the following changes in particle type: Inject a 2 mm, lightweight and a 2 mm, heavy (gold, tungsten, platinum). Position such that both particles are within a 1 cm^3 volume near the cell center with an initial center to center separation that lies in the range 0.3-0.5cm. (Not terminated as was in Experiment #5 and #6).

Experiment #8: (21 Holograms, five minutes of video) (Not isolated from ISS)

Repeat Experiment #1 except for the following:

1) Change in the fluid. Select a fluid such that the fluid density is the same as that of particle.
2) Include only the following cases:
   i) 60Hz., $\pm$200micron amplitude
   ii) 40Hz., $\pm$200micron amplitude
   iii) 80Hz., $\pm$100micron amplitude
3) Terminate experiment after step 9a.

Note: (7 holograms for each case)

Experiment #9: (84 Holograms, five minutes of video) (Not isolated from ISS)

1. Same as Experiment #2 except without isolation from ISS.

Note: The purpose of this experiment is twofold, to measure effects of ISS acceleration environment on the forced particle movement experiment and to measure the ISS acceleration environment. The light particle is used because the effects are expected to be the greatest for a lightweight particle. Also, the sensitivity of the acceleration measurement is greatest when a fluid/particle density ratio is much larger or much larger than unity.

Experiment #10: (34 holograms, five minutes of video) (Isolated from ISS)

Same as Experiment #2 with the following exceptions:

1) The two millimeter lightweight particle is to be injected in the near vicinity of a flat wall such that the surface of the wall and particle are separated by a distance that lies between 0.6-0.8 cm.
2) Terminate the experiment after step 8.

Note: The wall can be an existing cell wall or a wall that is added in the cell at any place. The purpose of this experiment is to observe wall effects on the particle movement.

Experiment #11: (84 holograms and 5 minutes of video) (Isolated from ISS)

Repeat Experiment #1, except for the particle type. Particle is to be TGS crystal of equivalent diameter 2 mm.

Experiment #12: (84 Holograms and five minutes of video) (Not Isolated from ISS)

Repeat Experiment #11 except not isolated from ISS.

Experiment #13: (26 holograms and five minutes of video) (Not isolated from ISS)

0.5 Degree centigrade/cm. temperature gradient normal to at least one optical axis.

Krytox filled cell.

1) Inject a 2 mm, polystyrene particle near cell center and retract injection device by at least one cm away from particle.
2) Record single pulsed hologram.
3) Advance film and store or down-link video frame.
4) Record a double-exposed hologram with 5-minute separation between pulses.
5) Advance film and store or down-link video frame.
6) Repeat the above cycle every ten minutes for two hours or until particle hits wall.

FLIGHT APPARATUS DESIGN

The flight apparatus is currently being designed by the NASA MSFC engineering team for SHIVA.

Figure 38 and **Figure 39** illustrate the preliminary instrument concept, which is based upon simplicity and reliability.

A laser diode will produce a diverging light that illuminates the test cell after collimation. As the light passes through the chamber, it will pick up particle and crystal profile information and in-line holograms will be recorded on 70 mm film. This ability will allow the particle's position to be precisely tracked, thus permitting the detection of very small motions.

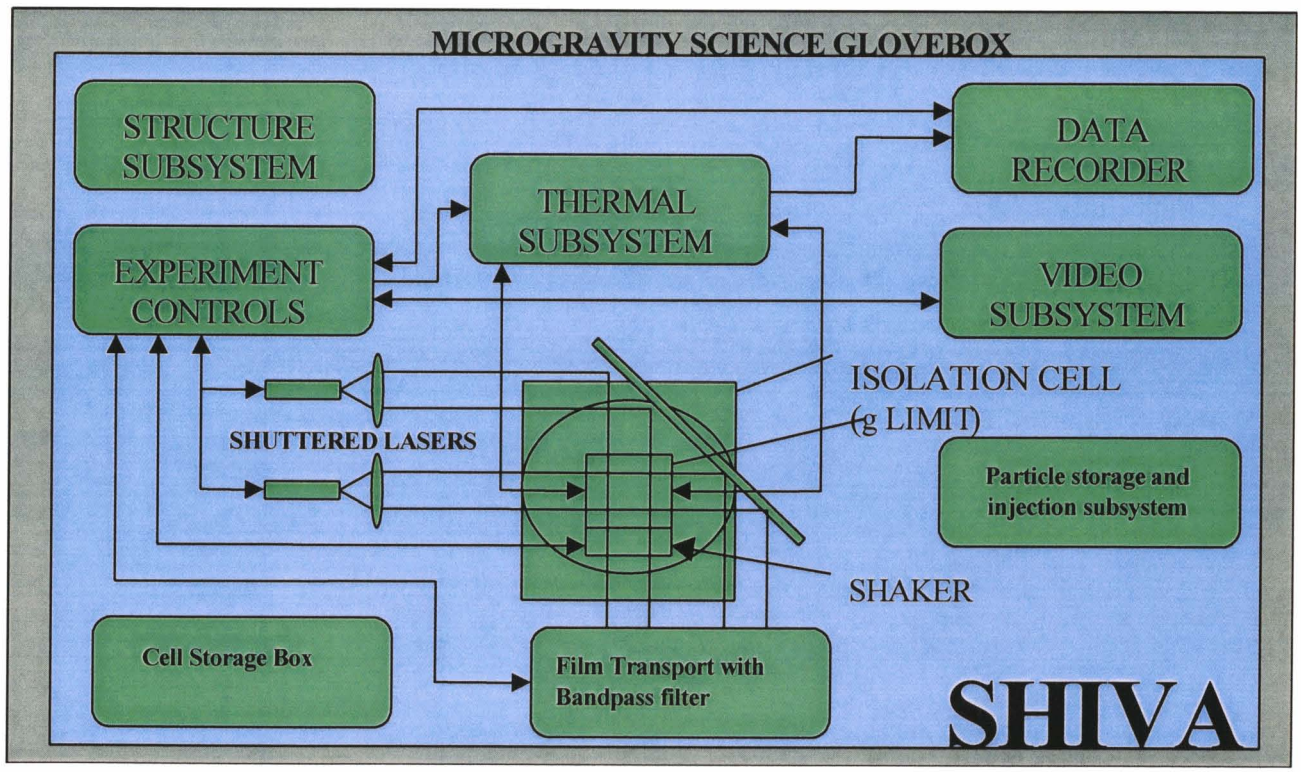

Figure 38. Spaceflight system concept.

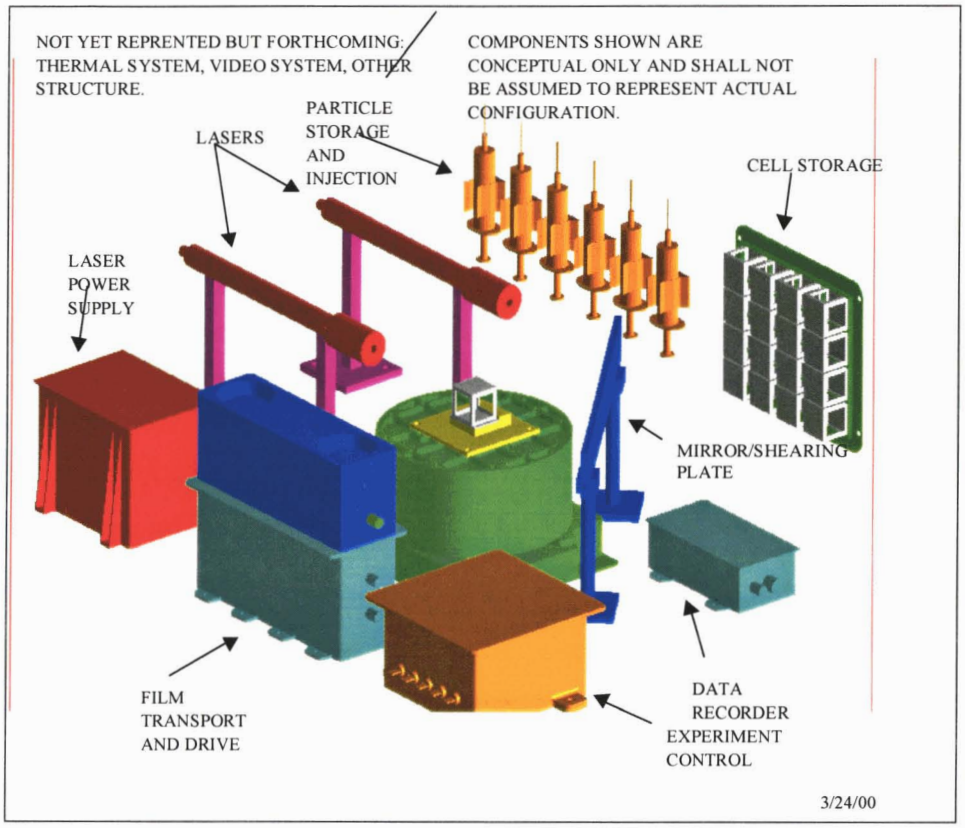

Figure 39. Perspective view of the flight hardware.

Figure 40 shows how the shearing plate is installed in the system. The wave shearing plate splits the beam that has passed through the test cell into two beams that are laterally shifted in space. The two beams interfere with each other providing a measurement of the gradient in phase across the wavefront. The wavefront that has passed through the depletion zone surrounding a particle will be interfered with a wave that is adjacent to the particle providing an infinite fringe interferogram of the depletion zone. The amount of the shift will be approximately 0.8 the thickness of the shear plate for glass. We require a shift of at least 0.5 centimeters. The shearing plate and the mirror can be formed on the same optical element for rigidity. The shear plate can be a piece of glass that is coated for 50% reflection on the first surface and 100% reflection on the second surface.

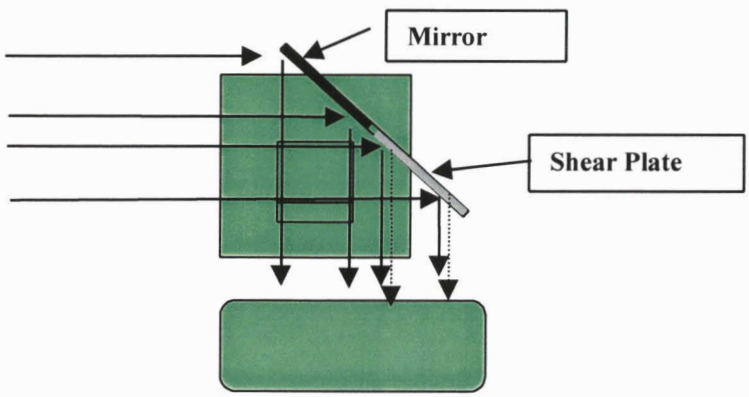

Figure 40. Wave shearing interferometer configuration.

The view containing the sheared wavefront should be normal to the direction of the temperature gradient.

CONCLUSIONS

The foregoing ground study has provided a solid foundation for a flight program. The study has demonstrated the benefit of recording data in the form of holograms and has resulted in a complete "tool kit" of methods for recording and analyzing holographic data. New observations of microgravity phenomena have been made for the first time. An important database has been produced by the study and this database is now available to other researchers. The database exists as a collection of CD ROMs and can be supplied to interested investigators upon request. A new solution to a fundamental equation of motion has been produced within the framework of the study, and this solution has predicted a wide range of interesting phenomena that can best be observed in microgravity. The study produced the beginning of an ongoing space flight definition program that has now progressed successfully to the second stage of requirements definition. Moving this research on to a space platform is the next step.

PUBLICATIONS ARISING FROM THE PROJECT

Journal

- C.F.M. Coimbra and R.H. Rangel "General Solution of the Particle Momentum Equation in Unsteady Stokes Flows", *J. Fluid Mech.*, 370, pp. 53-72 (1998).
- J.D. Trolinger, M. Rottenkolber, and F. Elandaloussi "Development and Application Of Holographic Particle Image Velocimetry Techniques For Microgravity Applications", *J. of Measurement Sciences and Technology*, Vol. 8 pp. 1573-1583 (1997).
- J.D. Trolinger, R.B. Lal, D. McIntosh and W.K. Witherow "Holographic Particle Image Velocimetry in the First International Microgravity Laboratory aboard the Space Shuttle Discovery", *Applied Optics*, Vol. 35, No. 4, pp. 681-689 (1 Feb. 1996).

Proceedings

- Carlos F.M. Coimbra, Roger H. Rangel, James D. Trolinger, "The Science Behind SHIVA:- Spaceflight Holography Investigation in a Virtual Apparatus" 39thAIAAAerospaceSciences, Meeting and Exhibit January 8-11, 2001 / Reno, NV
- J.D. Trolinger, M. Rottenkolber, W.K. Witherow and J. Rogers, "(SHIVA) Spaceflight Holography Investigation in a Virtual Apparatus", presented at the Tenth International Symposium On Applications Of Laser Techniques To Fluid Mechanics, Lisbon, Portugal July 10-13, 2000.
- James D. Trolinger, Roger H. Rangel, Carlos F.M. Coimbra, Ravindra B. Lal, William Witherow and Jan Rogers, SHIVA: Spaceflight Holography Investigation in a Virtual Apparatus, presented at the NASA Microgravity Material Sciences Conference, Huntsville, AL, June, 2000.
- James D. Trolinger, Roger H. Rangel, Carlos F.M. Coimbra, Ravindra B. Lal, William Witherow and Jan Rogers, SHIVA: Spaceflight Holography Investigation in a Virtual Apparatus AIAA 2000-0699,38th AIAA Aerospace Sciences Meeting and Exhibit January 10-13, 2000 / Reno, NV
- J.D. Trolinger, M. Rottenkolber, W.K. Witherow and J. Rogers, "(SHIVA) Spaceflight Holography Investigation in a Virtual Apparatus", AIAA 99-1032, 37th AIAA Aerospace Sciences Meeting, January 1999.
- C.F.M. Coimbra and R.H. Rangel "Spherical Particle Motion in Unsteady Viscous Flows", AIAA 99–1031 AIAA 99-1032, 37th AIAA Aerospace Sciences Meeting, January 1999.
- J.D. Trolinger, M. Rottenkolber, W.K. Witherow, and J. Rogers, "Holographic Particle Image Velocimetry Techniques for Microgravity Application", Paper No. AB105J, *Proceedings of VSJ-SPIE98*, December 6-9,1998, Yokohama, Japan.
- J.D. Trolinger, W.K. Witherow, J. Rogers, R.H. Rangel, C. Coimbra, and R.B. Lal, "Holographic Investigation of Transport Phenomena in a Virtual Spaceflight Chamber" Presented at the NASA Materials Science Conference, Huntsville Alabama, (July, 1998).
- J.D. Trolinger, R.H. Rangel, and R.B. Lal, "Particle Mechanics and G-jitter Observations in the IML-1 Spaceflight" AIAA 96-0504, 34th Aerospace Sciences Meeting, (January 1996).

Thesis

- C.F.M. Coimbra, (1998). "Unsteady Motion and Heat Transfer of Small Particles in Suspension," Ph.D. Dissertation - University of California, Irvine, 9.0.

REPORT DOCUMENTATION PAGE

Form Approved

PLEASE DO NOT RETURN YOUR FORM TO THE ABOVE ADDRESS

1. REPORT DATE *(DD-MM-YYYY)*	2. REPORT TYPE	3. DATES COVERED *(From – To)*
March 20, 2001	Final Report	06/04/96 to 12/03/00

4. TITLE AND SUBTITLE

Investigation of the Influence of Microgravity on Transport Mechanisms in a Virtual Spaceflight Chamber – A Ground-Based Program

5a. CONTRACT NUMBER
NAS8-408/48

5b. GRANT NUMBER

5c. PROGRAM ELEMENT NUMBER

6. AUTHOR(S)

Trolinger, James D, PhD

5d. PROJECT NUMBER

5e. TASK NUMBER

5f. WORK UNIT NUMBER

7. PERFORMING ORGANIZATION NAME(S) AND ADDRESS(ES)

MetroLaser, Inc., 18010 Skypark Circle Suite 100, Irvine, CA 92614-6428

8. PERFORMING ORGANIZATION REPORT NO.
TNM6JTF.doc

9. SPONSORING/MONITORING AGENCY NAME(S) AND ADDRESS(ES)

NASA George C. Marshall Spaceflight Center
ATTN: Pat Doty, SD44
Marshall SFC, AL 35812

10. SPONSOR/MONITOR'S ACRONYM(S)
COTR

11. SPONSOR/MONITOR'S REPORT NUMBER(S)

12. SUPPLEMENTARY NOTES

13. DISTRIBUTION/AVAILABILITY STATEMENT

14. ABSTRACT

The IML-1 Spaceflight produced over 1000 holograms of a well defined particle field in the low g Spacelab environment; each containing as much as 1000 megabytes of information. This project will further exploit this data and the concept of holographic storage of spaceflight to advance the understanding of convection in the space shuttle environment, g-jitter effects on crystal growth, and complex transport phenomena in low Reynolds number flows. The first objective of the proposed work is to advance the understanding of microgravity effects on crystal growth. This objective will be achieved through the use of existing holographic data recorded during the IML-1 spaceflight. The second objective is to design a spaceflight experiment that exploits the "virtual space chamber concept" in which holograms of space chambers can provide a virtual access to space.

15. SUBJECT TERMS

Holographic particle diagnostics, crystal growth, g-jitter

16. SECURITY CLASSIFICATION OF:			17. LIMITATION OF ABSTRACT	18. NUMBER OF PAGES	19a. NAME OF RESPONSIBLE PERSON
a. REPORT	b. ABSTRACT	c. THIS PAGE			Dr. James D. Trolinger
Unclassified	Unclassified	Unclassified	SAR	67	19b. TELEPHONE NUMBER *(Include area code)* (949) 553-0688, ext 225

Standard Form 298 (Rev. 8/98)
Prescribed by ANSI Std. Z39-18

AD33S 0 2
TURNER J/PUBLICATION
MARSHALL SPACE FLIGHT CENTER
HUNTSVILLE AL.

DELETIONS OR CHANGES 544-4494
RETURN ADDRESS AD33D
Document Code: 2444